MASTER

NUCLEAR ORIENTATION OF PRASEODYMIUM - 142

IN PRASEODYMIUM METAL

C.H. Smith and W. Weyhmann

Solid State and Low Temperature Physics Group

SCHOOL OF PHYSICS AND ASTRONOMY

FEBRUARY 1971

UNIVERSITY OF MINNESOTA
MINNEAPOLIS, MINNESOTA

DISCLAIMER

DISCLAIMER

Portions of this document may be illegible in electronic image products. Images are produced from the best available original document.

NUCLEAR ORIENTATION OF PRASEODYMIUM-142

IN PRASEODYMIUM METAL*

C. H. Smith and W. Weyhmann

Tate Laboratory of Physics

University of Minnesota, Minneapolis, Minnesota

ABSTRACT

The anisotropy of gamma radiation emitted by ^{142}Pr nuclei in polycrystalline praseodymium was measured in applied fields up to 41.7 kOe and temperatures down to 12 mK. The observed anisotropies were fitted to a model in which an appropriate powder average was taken of the electronic moments measured by Lebech and Rainford by neutron diffraction from a single crystal of praseodymium in applied fields. The Van Vleck moments calculated from the crystal field eigenfunctions and energy splittings of Bleaney do not provide a large enough internal field to cause the observed anisotropies.

In order to explain the large orientation observed, the first-forbidden beta decay of ^{142}Pr must be assumed to be almost pure Fermi with zero units of angular momentum usually carried away by the beta-neutrino pair.

ACKNOWLEDGEMENTS

We would like to acknowledge the assistance of the many people who have made this work possible. We would especially like to thank:

The excellent staff of the Physics Department without which not much would be accomplished around here;

Mr. Robert Swinehart for assisting in some of the data processing;

Mr. Javed Aslam, Mr. James Holliday, and the rest of the low temperature group who were always around when help was needed;

The University of Minnesota Computer Center and Macalester College for computer time.

One of us, C. H. Smith, would like to thank:

His wife, Meg, for her patient support through graduate school and also for typing and correcting this thesis;

Benjamin Smith for not arriving until after the typing was finished.

TABLE OF CONTENTS

LIST OF FIGURES

LIST OF TABLES

CHAPTER I

INTRODUCTION

Recently many investigations have been made of praseodymium metal to attempt to ascertain its magnetic structure and to understand the interactions which are responsible for it. The magnetic structure of the heavy rare earth metals, for which the exchange interactions are much larger than the splittings of the crystal field energy levels, are fairly well-known.[1] For the light rare earth metals, especially Pr and Nd, the crystal field splittings and the exchange energies are approximately equal, and theoretical predictions have not been entirely satisfactory in explaining experimental results. As an example measurements of the nuclear specific heat capacity of Pr metal[2,3] do not agree at all with Bleaney's calculations based on the crystal field levels.[4]

A further interesting aspect of Pr metal is that among the lanthanide elements with incomplete 4f shells, it is the only one whose specific heat capacity and bulk susceptibility do not indicate the onset of ordering at low temperatures. Whereas most rare earths have λ type anomalies in their specific heat, Pr has only a broad maximum at 35 K. This maximum has been associated with the population of the crystal field energy levels and has successfully been fitted using the crystal field levels given by Bleaney.[4,5] The curve of inverse susceptibility as a function of temperature extrapolates to a positive T intercept indicating possible ferromagnetic interactions, but the susceptibility becomes temperature

independent at low temperatures in a manner similar to that of a Van Vleck paramagnet.[6] This behavior as a Van Vleck paramagnet at low temperatures can be contrasted to the observation by neutron diffraction on polycrystalline Pr of lines corresponding to antiferromagnetic order with a Néel temperature of 25 K.[7] Even the neutron diffraction data is not conclusive. Recent neutron diffraction studies on single crystal Pr have failed to show antiferromagnetic ordering.[8,9]

Nuclear orientation studies offer a method of measuring the effective magnetic field experienced by the nuclei. We hoped that by measuring the orientation of ^{142}Pr in Pr metal we could learn more about the interactions and energy splittings. The orientation of the ^{142}Pr nuclei and, therefore, the internal field can be calculated by measuring the angular distribution of the γ radiation emitted by the ^{142}Pr nuclei.

In this thesis we will describe the orientation predicted by various models of the magnetic structure of Pr and compare them to our experimental data.

CHAPTER II

THEORY

Magnetic Structure of Praseodymium

Analysis of x-ray diffraction work on praseodymium has indicated that its equilibrium crystalline structure at room temperature is double-hexagonal close packed (dhcp).[10,11] In the dhcp structure single close packed layers of ions are stacked along the c axis in an ABAC sequence rather than the ABA sequence of hexagonal close packed (hcp) or ABC of face-centered cubic (fcc) structures. The dhcp structure is shown in Figure 1. The ratio of experimentally determined lattice constants, $c/a = 1.61$ for praseodymium, is very close to the ideal ratio for close packing of spheres, 1.633. Assuming the ideal close packing ratio, each ion has 12 nearest neighbors one lattice constant "a" distant -- 6 in its own layer and 3 each in the layers above and below. The ions in the A layer have nearest neighbors arranged the same as in a fcc lattice while the ions in B or C layers have nearest neighbors arranged the same as in an hcp lattice. The 6 second nearest neighbors which are $\sqrt{2}$ a distant are also arranged in fcc and hcp positions relative to the ions in the A and B or C layers respectively. The arrangement of the second nearest neighbors in fcc and hcp positions is easily justified if one notes that a second nearest neighbor is always in an adjacent layer. Third nearest neighbors and beyond do not necessarily match the fcc and

4
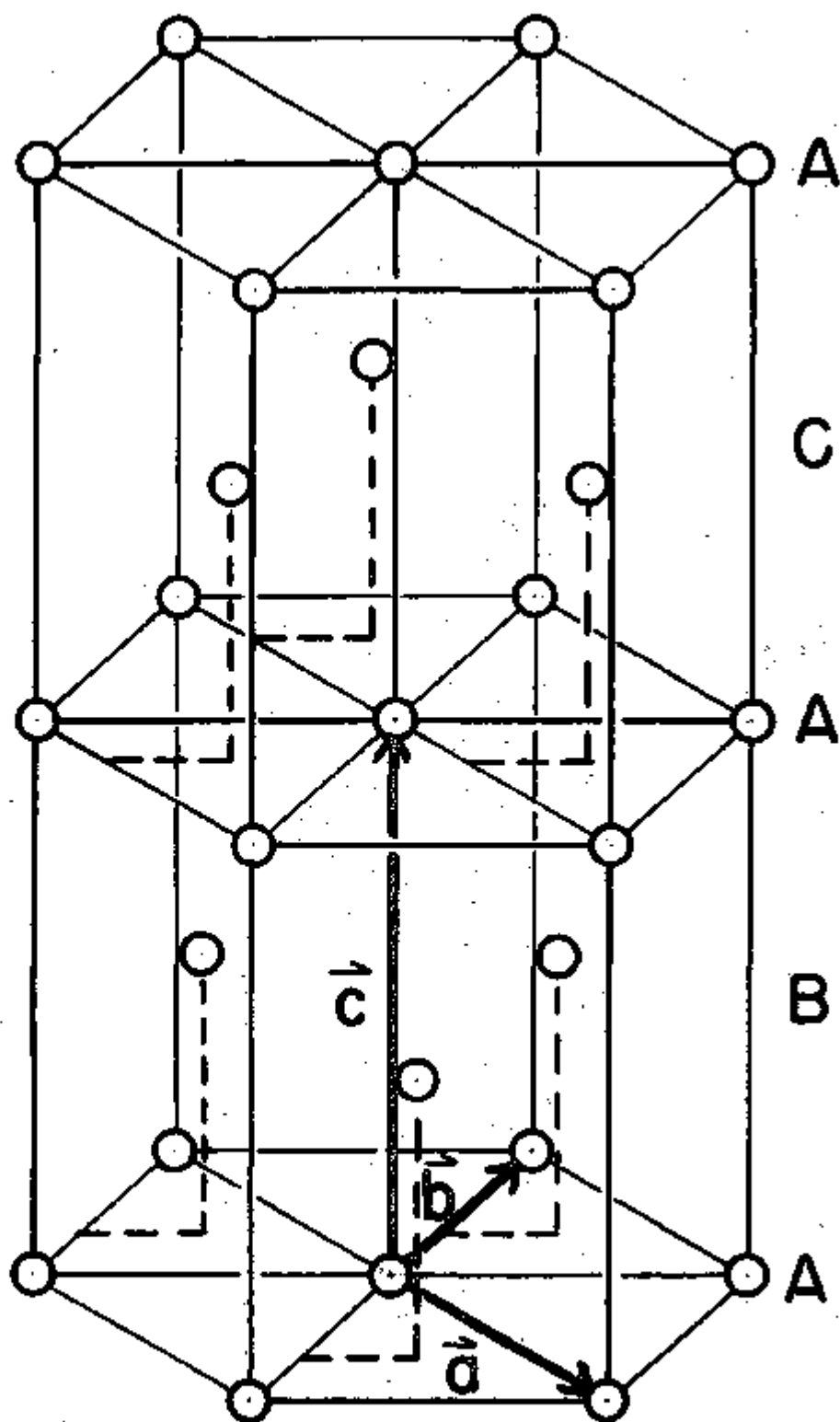
Figure 1. The double-hexagonal close packed
structure.

and hcp classifications, but their contributions to the crystal
field should be small and will be neglected. For crystal field
calculations we have two inequivalent sites -- one with a
hexagonal environment and one with a cubic environment.

Neutron diffraction data on polycrystalline praseodymium by
Cable et al. indicate the existence of antiferromagnetic ordering
below 25 K.[7] By comparing the results with work done on single
crystal neodymium,[12] the neighboring element on the periodic
chart, they tentatively suggest that praseodymium has a magnetic
structure with adjacent layers or every other layer aligned anti-
parallel but with a sinusoidal modulation of the moments in any of
the three equivalent $\underline{b}_1$ (100) directions in the reciprocal lattice.
The magnitude of the modulation wave vector is 0.13 b_1 and the
maximum moment is 0.7 μ_B per ion if all the moments participate or
1.0 μ_B per ion if only the moments on the cubic or hexagonal sites
align. The saturation moment for Pr^{3+} of 3.2 μ_B per ion apparently
does not develop on the antiferromagnetic sites.

Recent measurements of low temperature properties of Pr have
been successfully explained using the magnetic structure inferred
from the neutron diffraction work on polycrystalline samples.
Experiments on the nuclear specific heat of Pr in the temperature
range 0.02 to 0.4 K by Holmström et al. have indicated strong
support of a sinusoidally modulated antiferromagnetic ordering of
the moments on half the sites.[3] Their value for the maximum
moment, 0.95 μ_B, is in very close agreement with the value from
neutron diffraction. Nagasawa and Sugawara conclude from

resistivity, magnetoresistance, and magnetic susceptibility studies of Pr and its dilute alloys that there is no magnetic moment on the cubic site at low temperatures and a sinusoidal arrangement of moments on the hexagonal sites.[13]

Single crystal praseodymium has recently become available, and neutron studies have been started. Johansson et al. report no evidence of magnetic ordering in single crystal Pr at 4.2 K.[8] The lack of antiferromagnetic ordering in single crystal Pr and its occurence in polycrystalline Pr has been confirmed by Lebech and Rainford.[9] Johansson et al. attribute the antiferromagnetic ordering in polycrystalline Pr to the modification of the crystal field splittings by strains allowing the exchange interaction to dominate and cause spontaneous ordering. If the exchange and crystal field interactions are so closely balanced as to allow antiferromagnetic ordering in a polycrystalline sample and not in a single crystal, we can expect that modifying the crystal field splittings by applying an external field to a polycrystalline sample may also destroy the antiferromagnetic order.

Johansson et al. found that an applied field in the b_2 or (110) direction resulted in a large induced moment on both sites. They were able to separate the contributions from the moments on each site and found at 4.2 K and 46 kOe a moment of 1.8 μ_B per ion on the hexagonal site and 0.9 μ_B per ion on the cubic site. The total moment at 4.2 K showed definite curvature above 10 kOe indicating approach to saturation.

Lebech and Rainford also found a large induced moment on both
the hexagonal and cubic sites for applied fields in the (110)
direction. Due to a lack of change in the intensities of
reflections in the (100) and (104) directions whose structure
factors contain the combination $(2\mu_c - \mu_h)$, they conclude that the
moment on the hexagonal site is twice the moment on the cubic
site. Using their data together with the magnetization data of
Johansson et al. they derive the induced moments on the hexagonal
and cubic sites as functions of the applied field in both the
(001) and (110) directions. Figure 2 shows their results.

An additional complication to the magnetic structure of Pr
is the possible admixture of regions of the high temperature fcc
phase. Bucher et al. quench cooled Pr from above its transfor-
mation point of about 800 ^{0}C and were able to retain the fcc
phase at room temperature and below.[14] They measured a ferromagnetic
Curie temperature of 8.7 K and suggest that the presence of regions
of ferromagnetic fcc Pr could explain the small specific heat
anomaly at 3.2 K,[2] anomalously high hyperfine specific heat,[2,15]
and too large magnetic susceptibilities[4,5,6,16] found by other
workers. Fortunately our samples were foils and since cold
working was found to convert the fcc to the stable dhcp phase,[14]
it is doubtful that any fcc phase could have remained in our
samples.
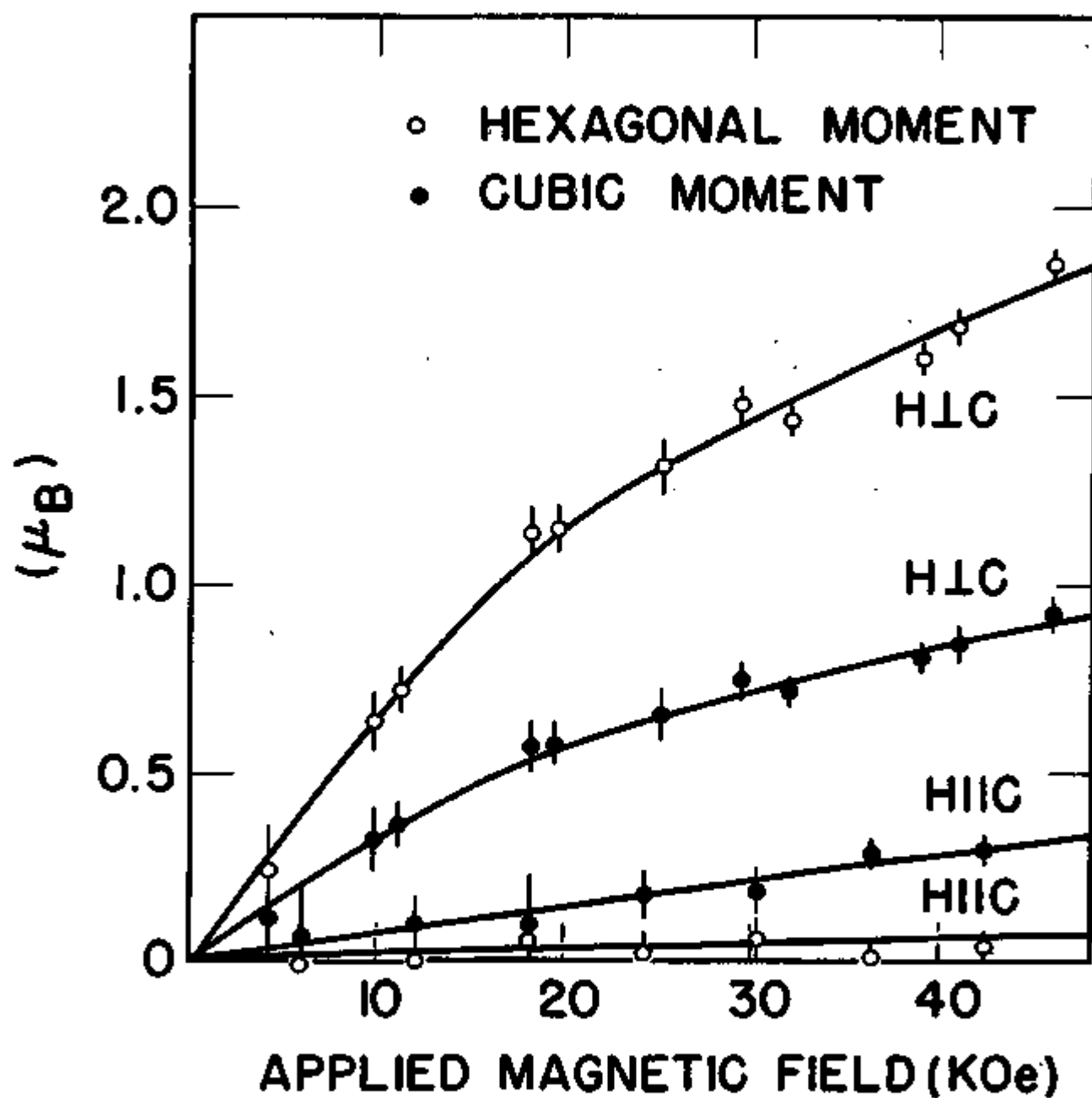
Figure 2.   Induced moments on hexagonal and cubic sites of Pr
for applied fields in the $\underline{b}_2$ (H⊥C) and $\underline{b}_3$ (H‖C) directions.
Graph taken from neutron diffraction work by Lebech and
Rainford.[9]

Crystal Field

Praseodymium metal, like most of the lanthanide metals, is usually described as tri-positive ions in a sea of conduction electrons. The ground state of the Pr^{3+} ion has two 4f electrons to which Hund's rules assign the state $^3H_4$. J is a good quantum number for these electrons buried fairly deeply in the ion, and the crystal field causes a Stark splitting of the $2J+1 = 9$ electronic levels. Bleaney has calculated the energy levels and states for both cubic and hexagonal fields.[4] The cubic field splits the electronic levels into a singlet ground state, a doublet, and two triplets. The hexagonal field splits them into a singlet ground state, two other singlets, and three doublets. The energy splittings were fit to the specific heat data of Parkinson et al.[17] A slightly better fit to this data has been made by Wallace et al. including the effect of a magnetic field on the eigenfunctions.[5] Bleaney's eigenfunctions and both sets of energy splittings are given in Table 1. We have corrected what we believe was a typographical error in Bleaney's work by changing $|\pm2>$ in the states for the cubic sites to $|\mp2>$. Without this change the states are not orthogonal. Grover also makes the same change in the first triplet state for a cubic field in Pr.[18]

Hyperfine Field

The interaction between a nucleus and the spin and orbital angular momenta of the electrons often can be represented as the nuclear magnetic moment interacting with a hyperfine field. This field is the magnetic field seen by the nucleus arising from

the angular momentum of all the electrons. We will only discuss here the details which apply to praseodymium metal. For a complete discussion of hyperfine interactions the reader is referred to the review article by Freeman and Watson.[19]

The hyperfine field in metallic Pr can have contributions both from the bound electrons in the Pr^{3+} ion and from the conduction electrons. The orbital angular momentum of the two 4f electrons is not quenched as it is for 3d and 4d transition ions. Therefore it contributes a major portion of the hyperfine field. This contribution to the hyperfine field, $\vec{H}_{orb}$, has been estimated by Kondo for Pr^{3+} to be:

$$\vec{H}_{orb} = 850 \ \vec{J} \ kOe \qquad\qquad II-1$$

where J is the angular momentum of the electronic state in units of $\hbar$.

The 4f electrons can also polarize the core s electrons which in turn can interact with the nuclei via the Fermi contact interaction. The core polarization contribution, $\vec{H}_{cp}$, has been estimated by Watson and Freeman to be:

$$\vec{H}_{cp} = -90 \ (g_J-1) \ \vec{J} \ kOe \qquad\qquad II-2$$

for any rare-earth ion.[21] Here (g_J-1) is the projection of the spin angular momentum $\vec{S}$ along $\vec{J}$. The gyromagnetic ratio, g_J, for Pr^{3+} is 4/5; therefore, the core polarization term is much smaller than the orbital term.

The third contribution to the hyperfine field is due to the Fermi contact interaction with the conduction electrons which are polarized by s-f exchange with the 4f electrons on the Pr^{3+} ions. For the rare earths typical contact terms in the hyperfine field are of the order of a few hundred kOe.[22] This term includes both core polarization and conduction electron contributions. The conduction electron contribution to the hyperfine field of Gd^{3+} is about 100 kOe.[23] If we assume the conduction electron term for Pr^{3+} is of the same order, we can neglect it in comparison to the orbital term which for a free Pr^{3+} ion is 3.4 MOe. For all of the rare earths the electrons which contribute to the magnetic properties are buried quite deeply in the 4f shell. The dominance of the spin and orbital terms in the hyperfine field together with the protected nature of the 4f electrons in the rare earths result in electron wave functions and interaction parameters in the rare earth metals which are very similar to those for free ions in their salts.

Both orbital and core polarization terms are proportional to $<J>$ -- the calculation of which using the crystal field energy levels and eigenfunctions together with perturbation theory is particularly simple for an experiment done at low temperature. The first excited electronic energy levels are 26 K and 90 K above the ground state for the hexagonal and cubic sites respectively; therefore, only the ground state will be populated at liquid helium temperatures. The expectation value of J in either singlet ground state is zero in the absence of an applied magnetic field

as can be easily verified from the eigenfunctions in Table 1. The interaction of an external field with the electron moments can be treated as a perturbation to the crystal field levels. The perturbed ground state in an applied field has an admixture of the first excited state and <J> is no longer zero. As a perturbation Hamiltonian we take the interaction of the magnetic dipole moment of the $^4H_3$ state with an external field H_o:

$$\mathscr{H}' = - g_J \mu_B \vec{J} \cdot \vec{H} \qquad \text{II-3}$$

where μ_B is the Bohr magneton. Expanding the dot product in terms of angular momentum raising and lowering operators and similar combinations of the x and y components of H_o we have

$$\mathscr{H}' = - g_J \mu_B \{H_z J_z + (H^+ J^- + H^- J^+)/2\} \qquad \text{II-4}$$

Using first order perturbation theory to find a new ground state, we can calculate the expectation value of J in the new ground state for both cubic and hexagonal sites. For the cubic site we find that

$$<J>_c = - \frac{(40/3)\ g_J \mu_B H_o/\Delta_c}{1 - (20/3)(g_J \mu_B H_o/\Delta_c)^2} \qquad \text{II-5}$$

The energy splitting to the first excited state has been written Δ_c. For the cubic site J is anti-parallel to H_o irrespective of the direction of the principal axes of the crystal. Therefore, we may take the z axis as the direction of the applied field and $<J>_c = <J_z>_c$. In the hexagonal site only the z component of J has

	Eigenstate Bleaney[4]	Energy (in K) Bleaney[4]	Energy (in K) Wallace[5]
CUBIC SITES			
triplet	$\sqrt{14/27}\|{\pm}4\rangle \pm \sqrt{25/54}\|{\pm}1\rangle - \sqrt{1/54}\|{\mp}2\rangle$ $\sqrt{7/54}\|{+}3\rangle - \sqrt{7/54}\|{-}3\rangle + \sqrt{20/27}\|0\rangle$	246	246
doublet	$\sqrt{7/27}\|{\pm}4\rangle \mp \sqrt{4/27}\|{\pm}1\rangle + \sqrt{16/27}\|{\mp}2\rangle$	150	154
triplet	$\sqrt{2/9}\|{\pm}4\rangle \mp \sqrt{7/18}\|{\pm}1\rangle - \sqrt{7/18}\|{\mp}2\rangle$ $\sqrt{1/2}\|{+}3\rangle + \sqrt{1/2}\|{-}3\rangle$	87	90
singlet	$\sqrt{10/27}\|{+}3\rangle - \sqrt{10/27}\|{-}3\rangle - \sqrt{7/27}\|0\rangle$	0	0
HEXAGONAL SITES			
doublet	$\|{\pm}4\rangle + 0.58z\|{\mp}2\rangle$	122	122
singlet	$\|0\rangle$	118	114
doublet	$\|{\pm}1\rangle$	106	105
doublet	$\|{\pm}2\rangle - 0.58z\|{\mp}4\rangle$	63	63
singlet	$\sqrt{1/2}\|{+}3\rangle + \sqrt{1/2}\|{-}3\rangle$	23	26
singlet	$\sqrt{1/2}\|{+}3\rangle - \sqrt{1/2}\|{-}3\rangle$	0	0

Table 1. Energy levels and eigenfunctions for Pr^{3+} ion in cubic and hexagonal fields. ($z = +0.22 \pm 0.02$)[4]

a non-zero expectation value; therefore, the z axis must be selected
as the c axis of the crystal:

$$\langle J \rangle_h = - \frac{18 \, g_J \mu_B H_z / \Delta_h}{1 - 9(g_J \mu_B H_z / \Delta_h)^2} \qquad \text{II-6}$$

Only H_z, the component of the applied field along the crystalline
axis, contributes to $\langle J \rangle_h$, so $\langle J \rangle_h$ is the same as $\langle J_z \rangle_h$ for this
case.

Since the orbital and core polarization terms are proportional
to $\langle J_z \rangle$, they can be combined. For reasons given above, the
proportionality should be the same for Pr metal as for a free Pr^{3+}
ion. Bleaney gives the hyperfine interaction for a free Pr^{3+} ion
in the form of the hyperfine Hamiltonian,

$$\mathcal{H} = - a \, \langle J_z \rangle \, m_I \qquad \text{II-7}$$

where a is the hyperfine constant and m_I is the magnetic quantum
number of the nucleus.[4] His value for a is 1093 ± 10 MHz.

The Hamiltonian for a nuclear dipole moment in an internal
field H_{int} along the z axis can be written

$$\mathcal{H} = - g_I \mu_N \, m_I H_{int} \qquad \text{II-8}$$

Here g_I is the nuclear gyromagnetic ratio and μ_N is the nuclear
magneton. Combining equations II-7 and II-8 we get

$$H_{int} = a \langle J_z \rangle / \, g_I \mu_N \qquad \text{II-9}$$

Using Bleaney's value for the hyperfine constant and appropriate

values for g_I and μ_N equation II-9 becomes .

$$H_{int} = 833 \langle J_z \rangle \text{ kOe} \qquad\qquad \text{II-10}$$

which is in very close agreement with Kondo's theoretical value
given in II-1. Using our calculated values for $\langle J_z \rangle$ we can
calculate the enhancement factor, the ratio of H_{int} to H_o. If
$g_J \mu_B H_o \ll \Delta$, or $H_o \ll 20$ kOe per Kelvin energy splitting, we can
ignore the denominators in II-5 and II-6 and obtain

$$H_{int} = - 597 \, H_o/\Delta_c \qquad\qquad \text{II-11}$$

for the cubic site and

$$H_{int} = - 806 \, H_o/\Delta_h \qquad\qquad \text{II-12}$$

for the hexagonal site where both of the splittings, Δ, are
expressed in Kelvins. The enhancement factors, then, are 6.6 for
a 90 K splitting on the cubic site and 31 for a 26 K splitting on
the hexagonal site.

The above values for the hyperfine fields at both sites
calculated from crystal field levels can be compared to the results
from neutron diffraction work on single crystals by noting that
the electronic moment on a site will be just

$$\vec{\mu} = - g_J \mu_B \, \vec{J} \qquad\qquad \text{II-13}$$

Using equation II-10 and the gyromagnetic ratio for Pr we can find
the relationship between the hyperfine field and the moment on the
site. If the moment is measured in units of Bohr magnetons,

$$H_{int} = - 1.04 \mu \text{ MOe}$$ II-14

For the linear portion of the graph in Figure 2 the slope indicates an enhancement factor of 68 for the hexagonal site and 34 for the cubic site -- far larger than the values from the perturbation calculations on the crystal field levels. Also departure from a linear behavior is noticeable by 20 kOe applied field -- far earlier than the denominator in the expression for $\langle J_z \rangle$ predicts. These differences indicate that either the energy splittings derived from specific heat data are incorrect or that the electronic moments on the sites cannot be calculated only from the moment induced by an external field on a crystal field ground state singlet.

Nuclear orientation can be used as a probe to determine the hyperfine field seen by the nuclei. It should, therefore, make a good test to determine whether the hyperfine field determined from the crystal field energy levels and eigenfunctions or that from neutron diffraction work is correct.

Thermal Equilibrium Nuclear Orientation

A spatial ordering of nuclear spins can be achieved by several methods. For the reader interested in general nuclear orientation many review articles and books exist.[24,25,26,27] In this section we will describe only the orientation of nuclei in thermal equilibrium with their surroundings.

Thermal equilibrium nuclear orientation utilizes some interaction which lifts the degeneracy of the 2I+1 magnetic sublevels of the nuclei, $m_I = -I, -I+1, \ldots, +I$, and low temperatures to preferentially populate the lowest energy levels. (The subscripted I on the m will be dropped for the rest of this section.) The population, a_m, of the _m_th state in a statistical ensemble is given by the Boltzmann distribution

$$a_m = \exp(-E_m/kT)/\sum_m \exp(-E_m/kT) \qquad \text{II-15}$$

where E_m is the energy of the _m_th sublevel and k is Boltzmann's constant. If the degeneracy between states with the same value of $|m|$ is lifted, the system can be polarized. If the degeneracy between states with the same value of $|m|$ is not lifted, but the degeneracy between at least some states of different $|m|$ is lifted, the system can be aligned. An aligned system does not distinguish between +z and -z.

The amount of orientation is often expressed in the form of the orientation parameters $f_k(I)$. These parameters are 2I independent linear combinations of the _n_th moments, $\sum_m m^n a_m$, of the populations of the 2I+1 magnetic sublevels. The 2I $f_k(I)$'s uniquely specify the orientation of an ensemble of nuclei just as 2I of the normalized a_m's do. The normalization equation $\sum_m a_m = 1$ supplies the remaining condition. The orientation parameters are defined in Cox and Tolhoek.[28] The ones most often used are:

$$f_1 = I^{-1} \sum_m a_m m \qquad\qquad \text{II-16}$$

$$f_2 = I^{-2} \sum_m a_m (m^2 - I(I+1)/3) \qquad\qquad \text{II-17}$$

$$f_4 = I^{-4} \sum_m a_m (m^4 - m^2(6I^2+6I-5)/7$$
$$+ \frac{3}{35} I(I+1)(I-1)(I+2)) \qquad\qquad \text{II-18}$$

In a polarized system one or more of the "odd" f_k's are non-zero
while in an aligned system, one in which $a_m = a_{-m}$, one or more of
the "even" f_k's are non-zero and all of the "odd" ones are zero.

Directional Distribution of γ Radiation

The amount of orientation in an ensemble of radioactive nuclei
is often measured by observing the directional distribution of γ
radiation. The intensity of γ radiation is symmetric about the
z axis which is determined by the internal field seen by the
nuclei. In a polycrystalline sample the z axis can be taken as the
direction of an applied magnetic field. In a single crystal
sample any preferred crystalline axis must be aligned with the
external field in order to use the external field to determine
the axis of symmetry. The intensity at an angle θ to the z axis
can be expanded in terms of the Legendre polynomials $P_k(\cos\theta)$:

$$W(\theta) = \sum_k D_k(I) f_k(I) P_k(\cos\theta) \qquad\qquad \text{II-19}$$

The angular momentum properties of the γ transition are included
in the D_k's, and the amount of orientation is given by the f_k's
which have already been discussed. The D_k's are quite simple

for pure dipole and quadrupole transitions. If the initial spin of the nucleus and the spin after the γ transition are given by I_i and I_f respectively we can write:

Dipole Radiation

$$I_f = I_i-1, \quad W(\theta) = 1 + (3/2)N_2(I_i)f_2(I_i)P_2(\cos\theta) \qquad \text{II-20}$$

$$I_f = I_i, \quad W(\theta) = 1 - (3/2)K_2(I_i)f_2(I_i)P_2(\cos\theta) \qquad \text{II-21}$$

$$I_f = I_i+1, \quad W(\theta) = 1 + (3/2)M_2(I_i)f_2(I_i)P_2(\cos\theta) \qquad \text{II-22}$$

Quadrupole Radiation

$$I_f = I_i-2, \quad W(\theta) = 1 - (15/7)N_2(I_i)f_2(I_i)P_2(\cos\theta)$$
$$- 5\ N_4(I_i)f_4(I_i)P_4(\cos\theta) \qquad \text{II-23}$$

$$I_f = I_i+2, \quad W(\theta) = 1 - (15/7)M_2(I_i)f_2(I_i)P_2(\cos\theta)$$
$$- 5\ M_4(I_i)f_4(I_i)P_4(\cos\theta) \qquad \text{II-24}$$

In the equations above the D_k's have been replaced by their specific forms for the various transitions:

$$N_2(I) = I/(2I-1) \qquad \text{II-25}$$

$$K_2(I) = I/(I+1) \qquad \text{II-26}$$

$$M_2(I) = I^2/(I+1)(2I+3) \qquad \text{II-27}$$

$$N_4(I) = I^3/(I-1)(2I-1)(2I-3) \qquad \text{II-28}$$

$$M_4(I) = I^4/(I+1)(I+2)(2I+3)(2I+5) \qquad \text{II-29}$$

Expressions for higher multipolarity transitions and for mixed dipole and quadrupole radiations can be found in the literature.[26,29]

Because half lives for γ emission are usually extremely
short, a parent nucleus with a half life long enough to
allow assembly and cooling of the apparatus must be chosen
unless the isotope to be studied is produced in the apparatus.
The parent nucleus β decays to a short-lived excited state of a
daughter nucleus which in turn decays by a γ transition or a
γ cascade to its ground state. Figure 3 shows such a decay.
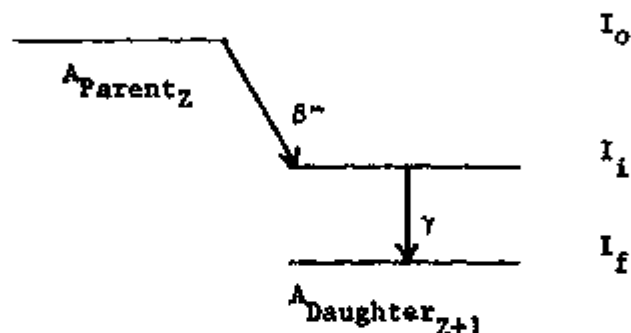
Figure 3. β decay of a parent nucleus with spin
I_0 to an excited state of a daughter nucleus
followed by a γ transition, $I_i \rightarrow I_f$, to its
ground state.

·Since the half lives for γ emission are usually much shorter
than the thermal relaxation time to the surrounding lattice
or to the conduction electrons, there is no thermal reorientation
of the daughter nucleus before it γ decays. There may, however,
be reorientation due to the angular momentum properties of the
β transition. If the β-ν pair carries off no angular momentum,
the a_m's for the daughter are the same as for the parent.

If, however, the lepton pair carries off angular momentum, there must be reorientation between the parent and daughter nuclei. We can take this reorientation into account in our expression for $W(\theta)$ by writing the orientation of the initial state as the product of the orientation of the parent state times an attenuation coefficient, B_k, which depends upon the spins of the parent and the daughter and L, the angular momentum carried off by the $\beta-\nu$ pair:

$$W(\theta) = \sum_k D_k(I_i) B_k(I_o, I_i, L) f_k(I_o) P_k(\cos \theta) \qquad II\text{-}30$$

The same attenuation parameters can be used to account for a preceding γ transition in a cascade where L is now the angular momentum of the γ radiation or 2L is the multipolarity of the transition. The attenuation parameters can be determined using Racah algebra.[30]

$$B_k(I_o, I_i, L) = (2I_o+1) W(I_i L k I_o; I_o I_i) w_k(I_i) / w_k(I_o)$$

$$II\text{-}31$$

where $W(I_i L k I_o; I_o I_i)$ is a Racah coefficient and

$$w_k(I) = \binom{2k}{k}^{-1} I^{-k} \left[\frac{(2I+k+1)!}{(2k+1)(2I-k)!} \right]^{\frac{1}{2}} \qquad II\text{-}32$$

An introduction to Racah coefficients is given by Rose.[31] Using tables of Racah coefficients calculated by Beidenharn et al.[32] we can calculated the B_k's for a few simple cases:

For transitions $I_0 \to I_1 = I_0 \pm L$

$$B_k(I_0, I_0 \pm L, L) = D_k(I_0)/D_k(I_1) \qquad \text{II-33}$$

For transitions $I_0 \to I_1 = I_0$ and $L = 1$

$$B_k(I_0, I_0, 1) = 1 - k(k+1)/2I_0(I_0+1) \qquad \text{II-34}$$

For transitions $I_0 \to I_1 = I_0$ and $L = 2$

$$B_k(I_0, I_0, 2) = \frac{3\,A(A+1) - (4/3)I_0^2(I_0+1)^2}{I_0(2I_0+3)(2I_0+2)(2I_0-1)} \qquad \text{II-35}$$

where

$$A = k(k+1) - 2I_0(I_0+1) \qquad \text{II-36}$$

For further cases see the article by Fano.[30] If the lepton pair does not always carry off the same amount of angular momentum, a sum of the appropriate B_k's multiplied by the probability, α_L, of a given value of L must be used.

First-Forbidden Beta Decay

The beta transition which is of interest to us is a $2^- \to 2^+$ first-forbidden β decay. There are six overlap integrals or nuclear matrix elements which can contribute to such a $2^- \to 2^+$ decay. These matrix elements are of rank $\lambda = 0$, 1, and 2, where the rank of the matrix element is equal to the angular momentum carried off by the $\beta-\nu$ pair. The matrix elements are given below in the notation of Kotani:[33,34]

$$zw = C_A \int \vec{\sigma} \cdot \vec{r} \qquad \lambda = 0 \qquad \text{II-37}$$

$$zv = C_A \int i \gamma_5 \qquad \lambda = 0 \qquad \text{II-38}$$

$$zu = C_A \int i(\vec{\sigma} \times \vec{r}) \qquad \lambda = 1 \qquad \text{II-39}$$

$$zy = -C_V \int i \alpha \qquad \lambda = 1 \qquad \text{II-40}$$

$$zx = -C_V \int \vec{r} \qquad \lambda = 1 \qquad \text{II-41}$$

$$z = C_A \int B_{ij} \qquad \lambda = 2 \qquad \text{II-42}$$

where the matrix elements have been written in terms of the
unique one, II-42. For a complete treatment of first-forbidden
β decay see the review article by Weidenmüller.[35] A set of
equations specialized to $2^- \to 2^+$ first-forbidden β transitions
followed by $2^+ \to 0^+$ electric quadrupole (E2) γ transitions can be
found in an article by Pipkin et al.[36] It is with just such
transitions we will be concerned.

Many $2^- \to 2^+$ first-forbidden β transitions can be adequately
described by the ξ approximation.[33,34,37] The ξ approximation
involves retaining the lead term in an expansion of the
relativistic lepton wave function in the Coulomb field of the
daughter nucleus in descending powers of the parameter ξ which is
one-half of the Coulomb energy of an electron located at the
nuclear radius:

$$\xi = \alpha Z / 2R \qquad \text{II-43}$$

where α is the fine structure constant, Z is the charge on the
daughter nucleus, and R is the nuclear radius in electron
Compton wavelengths. This approximation should be valid for
nuclei with Z>20 if the maximum kinetic energy of the electron
emitted is much less than ξ.[38] In the ξ approximation the matrix
elements given in II-37 through II-42 are small compared to the
linear combination V and Y:

$$V = v + \xi w \qquad\qquad \lambda = 0 \qquad\qquad\qquad II\text{-}44$$

$$Y = y - \xi(u + x) \qquad\qquad \lambda = 1 \qquad\qquad\qquad II\text{-}45$$

Therefore, the observable quantities are expressed in terms of
V and Y. Some of the characteristics of first-forbidden
β transitions which obey the ξ approximations are: a spectrum
whose shape correction factor C(W) is energy independent,[38]
small values for the β-ν directional correlation coefficient,[37]
and log ft values in the range 7.5 ± 1.5.[39] Generally the
observable quantities in a first-forbidden β transition which
satisfies the ξ approximation show characteristics which are
similar to those of allowed transitions with the Fermi and the
Gamow-Teller matrix elements replaced with V and Y respectively.[38]
Since Fermi selection rules correspond to the electron and
neutrino having spins antiparallel, V corresponds to the lepton
pair carrying away zero angular momentum. Similarly the
Gamow-Teller selection rules correspond to the spins parallel or
one unit of lepton angular momentum. The matrix element z

corresponding to two units of angular momentum carried off by the $\beta-\nu$ pair is very small; therefore, we can set $\alpha_2 = 0$ and $\alpha_0 + \alpha_1 = 1$. We can now calculate the attenuation coefficients for a $2^- \rightarrow 2^+$ β decay described by the ξ approximation as a sum of terms from equations II-33, II-34, and II-35 multiplied by the appropriate σ_L's and, by using the above restrictions on the α_L's express these attenuation coefficients in terms of α_1:

$$B_2 = 1 - \alpha_1/2 \qquad \qquad \text{II-46}$$

$$B_4 = 1 - 5\alpha_1/3 \qquad \qquad \text{II-47}$$

By making the ξ approximation in the expressions for α_0 and α_1 found in the article by Pipkin et al.,[36] we find that α_0 is proportional to V^2 and α_1 is proportional to Y^2 with the same proportionality constant. Therefore,

$$\alpha_0/\alpha_1 = V^2/Y^2 \qquad \qquad \text{II-48}$$

$$\alpha_1 = 1/(1 + V^2/Y^2) \qquad \qquad \text{II-49}$$

Orientation of ^{142}Pr in Praseodymium Metal

^{142}Pr is formed by the irradiation of ^{141}Pr, the only stable isotope of praseodymium, with thermal neutrons. It β decays with a 19.2 hour half life to ^{142}Nd in its ground state 96.3% of the time. The remaining 3.7% of the decays are first-forbidden β decays to an excited state of ^{142}Nd followed by a 1.57 MeV electric quadrupole (E2) γ transition to the ground

state. The decay scheme is shown in Figure 4. The data in the figure is taken from the 6th edition of Table of Isotopes.[40]

The first-forbidden β decay of ^{142}Pr has been studied by Hess et al.[41] They measured the shape factor of the β spectrum, the β-γ directional correlation, and the β-γ circular polarization correlation. They found a constant shape factor and a very small anisotropy of the β-γ directional correlation. These indications together with the ft value (log ft = 7.1) are evidence that the $2^- \rightarrow 2^+$ β transition should be adequately described by the ξ approximation.

The decay which we observed in this experiment was the γ transition $I_i = 2 \rightarrow I_f = 0$. The angular distribution of γ radiation can be calculated from equations II-23, II-25, II-28 and II-30 using $I_o = I_i = 2$:

$$W(\theta) = 1 - (10/7)B_2 f_2 P_2(\cos\theta)$$
$$- (40/3)B_4 f_4 P_4(\cos\theta) \qquad \text{II-50}$$

The f_k's are given in equations II-17 and II-18, and the B_k's can be calculated from II-46, II-47, and II-49 if the value of V/Y is known. The value of V/Y was found by Hess et al. to be either -0.2 or -2.7 from β-γ circular polarization correlation measurements. They preferred the first value on theoretical grounds. Using the error limits on V/Y set by Hess et al. we find:
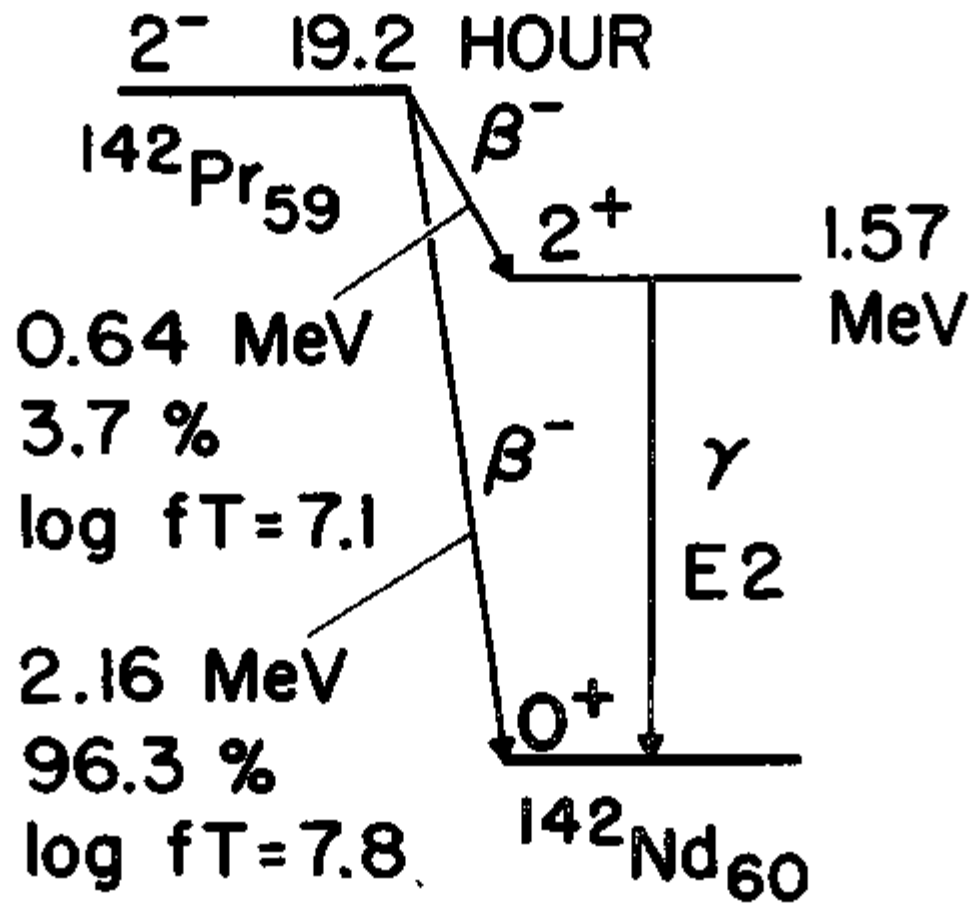
Figure 4. Nuclear decay scheme of ^{142}Pr.

$$V/Y = \qquad -0.2^{+0.05}_{-0.18} \qquad\qquad -2.7^{+0.9}_{-1.3}$$

$$B_2 = \qquad 0.519^{-0.018}_{+0.044} \qquad\qquad 0.940^{-0.058}_{+0.031}$$

$$B_4 = \qquad -0.602^{-0.060}_{+0.146} \qquad\qquad 0.800^{-0.193}_{+0.102}$$

The first possibility for V/Y corresponds to mostly
Gamow-Teller interactions and the second to mostly Fermi
interactions. For a pure Gamow-Teller interaction $B_2 = \tfrac{1}{2}$ and
for a pure Fermi interaction $B_2 = 1$.

Measurements of $\beta-\gamma$ circular polarization correlation do not
give a unique value for the ratio of the zero and first order
matrix elements for first-forbidden β decay described by the ξ
approximation. Nuclear orientation, by providing information
about the orientation of the nuclei following the β decay,
provides a means of selecting one of the two possible ratios.
Nuclear orientation measurements on ^{142}Pr implanted in an iron
host made by Ried et al. indicated that $(\alpha_0/\alpha_1)^2 \geq 0.25$ or
$(V/Y) \geq \tfrac{1}{2}$.[23] This value would indicate a preference for
$V/Y = -2.7$. Our data will be checked for compatibility with both
ratios.

We can now calculate the angular distribution of γ radiation
from oriented ^{142}Pr for the various possible models of
praseodymium metal. If the interaction which lifts the
degeneracy among the magnetic sublevels of the nuclei can be
written as the magnetic dipole moment of the nucleus interacting

with an internal field, H_{eff}, we can write the energy E_m in equation II-15 as

$$E_m = -g_N \mu_N \, m \, H_{int} \qquad\qquad \text{II-51}$$

where the axis of quantization has been taken along the effective field. The combination H_{int}/T now appears in the exponentials that determine the a_m's and the E_k's, so the orientation of the nuclei and hence the angular distribution of γ radiation is a function of H_{int}/T. $W(\theta)$, the intensity of γ radiation parallel to the z axis, is shown in Figure 5 as a function of H_{int}/T for both possible values of V/Y. The dependence shown is for a system in which all of the ^{142}Pr nuclei experience the same effective field. Praseodymium metal has two inequivalent sites with equal populations; therefore, we must take an average over both sites since they have different effective fields.

$$W(\theta) = \tfrac{1}{2}\{W(\theta)_c + W(\theta)_h\} \qquad\qquad \text{II-52}$$

The cubic and hexagonal contributions have been designated by appropriate subscripts. The effective field at each site can be obtained from either the calculations using crystal field splittings or from the electronic moments deduced from single crystal neutron diffraction studies. Since the models predict different results, they will be treated separately.
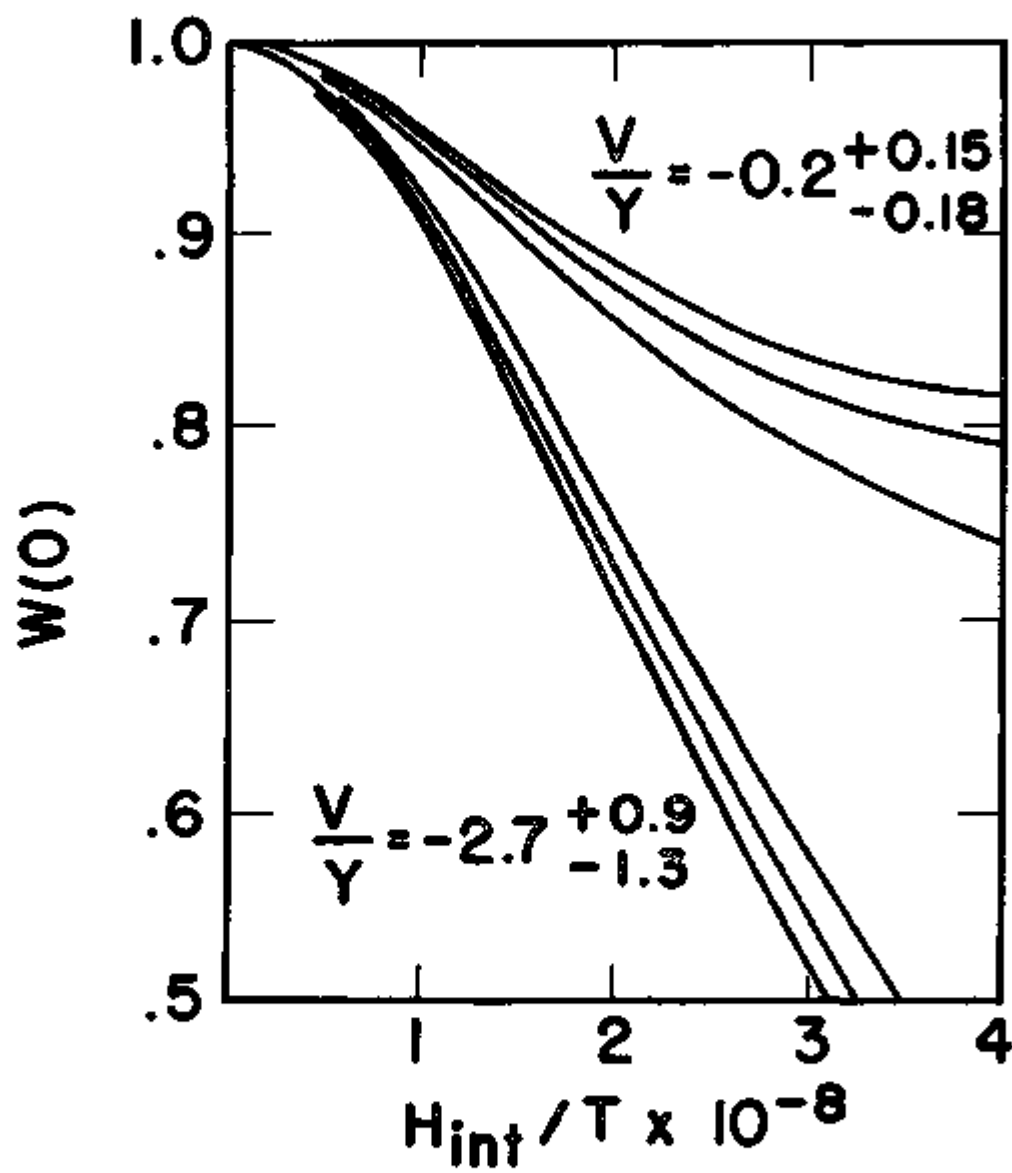
Figure 5. Intensity of γ radiation from ^{142}Pr
parallel to the applied field as a function
of H_{int}/T for $V/Y = -0.2$ and -2.7.

Crystal field splittings -- Since the energy of two
antiparallel spins in a magnetic field is not a function of their
orientation to the field direction, an applied field will not
orient an antiferromagnetic system unless the field is large
enough to disrupt the antiferromagnetic order by canting the spins.
Therefore, an antiferomagnetic crystal will remain oriented
with respect to the crystal axis rather than with respect to the
applied field except for very large applied fields. A polycrystal-
line antiferromagnetic sample should display no orientation since
the crystalline axes in the crystallites point in all directions
averaging out the orientation possessed by each crystallite. The
γ radiation from ^{142}Pr atoms in the hexagonal sites, therefore,
should be isotropic for a polycrystalline sample. Thus the total
orientation will result in a directional distribution of
γ-radiation intensity:

$$W(\theta) = \tfrac{1}{2}\{W(\theta)_c + 1\} \qquad\qquad II-53$$

The expectation value of $\vec{J}$ on the cubic site, and therefore
$\vec{\mu}$ and $\vec{H}_{eff}$, is parallel or antiparallel to the applied field;
hence due to the high symmetry of the cubic site, a polycrystalline
sample will produce the same radiation distribution as a single
crystal with its crystal axis parallel to the applied field.

If the antiferromagnetic alignment of the moments on the
hexagonal sites is destroyed by an applied field, then both
sites can contribute to $W(\theta)$. Since only the component of the

applied field along the crystalline axis contributes to $<J_z>$, for a polycrystalline sample we must take a powder average of contributions to $W(0)_h$ from crystallites with their c axes at all possible angles to the applied field. In an ideal hcp structure there are 8 equivalent (001) directions which can be taken as the c axis. Therefore we need only take the powder average over one octant of a sphere -- an octant centered about the (001) direction. The use of a computer makes the numerical calculation of $W(0)$ from a powder average relatively simple. The observed $W(0)$ is again just an average of the contributions from the hexagonal and cubic sites.

Neutron diffraction data -- The effective field experienced by the nuclei in the two sites can also be calculated by using equation II-14 and the electronic moments shown in Figure 2. If in a polycrystalline sample the hexagonal moments are antiferromagnetically aligned, we again have the situation described by equation II-53 with the hexagonal sites providing only an isotropic background. If the applied field changes the balance between exchange interaction and crystal field effects enough to make antiferromagnetic ordering unfavorable, both cubic and hexagonal contributions must be considered.

In Figure 2 it is obvious that there is a large directional anisotropy in the moment on the hexagonal site. Only the component along the $\underline{b}_2$ or (110) direction is significant. Since there are 12 equivalent (110) directions in an hcp lattice, a powder

average of W(0) must be taken over all possible crystallite directions in 1/12 sphere. Again this can be numerically calculated using a computer. It is very interesting to note that a significant electronic moment develops for the applied field perpendicular to the crystal axis rather than parallel to it as predicted by the calculations using the crystal field splittings.

There is also a much smaller anisotropy in the moment that develops on the cubic site. If $<\vec{J}>$ is antiparallel to $\vec{H}_0$ as was calculated using perturbation theory on the crystal field eigenfunctions, there would be no such anisotropy. Lebech and Rainford suggest that the anisotropy may be due to a non-ideal c/a ratio and exchange with neighbors which are in hexagonal sites.[9] The anisotropy of the cubic moment will decrease the deviation of $W(0)_c$ from unity compared to the isotropic case but not by as much as the extremely large hexagonal moment anisotropy causes $W(0)_h$ to deviate. Also the contribution to $W(0)$ from the cubic sites is smaller than that from the hexagonal sites due to the smaller moment on the cubic site. Therefore, we will not perform a powder average on the contributions to $W(0)_c$ but assume that the the cubic site acts almost as a single crystal. The appropriate powder average is quite involved requiring the averaging of contributions to $W(0)_c$ caused by the resultant moment due to both the moment along $\underline{b}_2$ and along $\underline{b}_3$ averaged over all possible directions of $\underline{b}_2$ in 1/12 sphere and for each $\underline{b}_2$, all possible directions of the particular $\underline{b}_3$ that is most nearly parallel to H_0.

We can now compare the experimentally measured values of $W(0)$ to those predicted by these models of oriented ^{142}Pr in praseodymium metal.

CHAPTER III

EXPERIMENTAL APPARATUS AND PROCEDURE

Cryostat

The adiabatic demagnetization cryostat used for cooling the
sample has been discussed in detail elsewhere.[42] Only a brief
description will be included here. A block diagram of the
cryostat, dewars, and pumps showing the temperatures achieved
by each section is pictured in Figure 6. The sample is cooled by
a paramagnetic salt which is demagnetized from an initial
temperature of 0.3 K and an initial field of 18 kOe to a final
temperature of about 10 mK. The sample is soldered to copper
fins which are imbedded in the salt pill containing about 300 cm^3
of a slurry of powdered chrome alum mixed with a solution of half
glycerine and half saturated aqueous solution of chrome alum.

A schematic diagram of the cryostat is shown in Figure 7.
For clarity the liquid nitrogen dewar is not included. The
superconducting magnets for polarizing the sample and for
saturating the paramagnetic salt are located in the liquid
helium bath at 4.2 K. The ^{4}He and ^{3}He evaporators at 1 K and
0.3 K respectively are isolated from the liquid helium bath by a
vacuum can. Gaseous ^{3}He returning to the evaporator is liquified
by a condenser in thermal contact with the ^{4}He evaporator which
is filled from the helium bath through a needle valve and
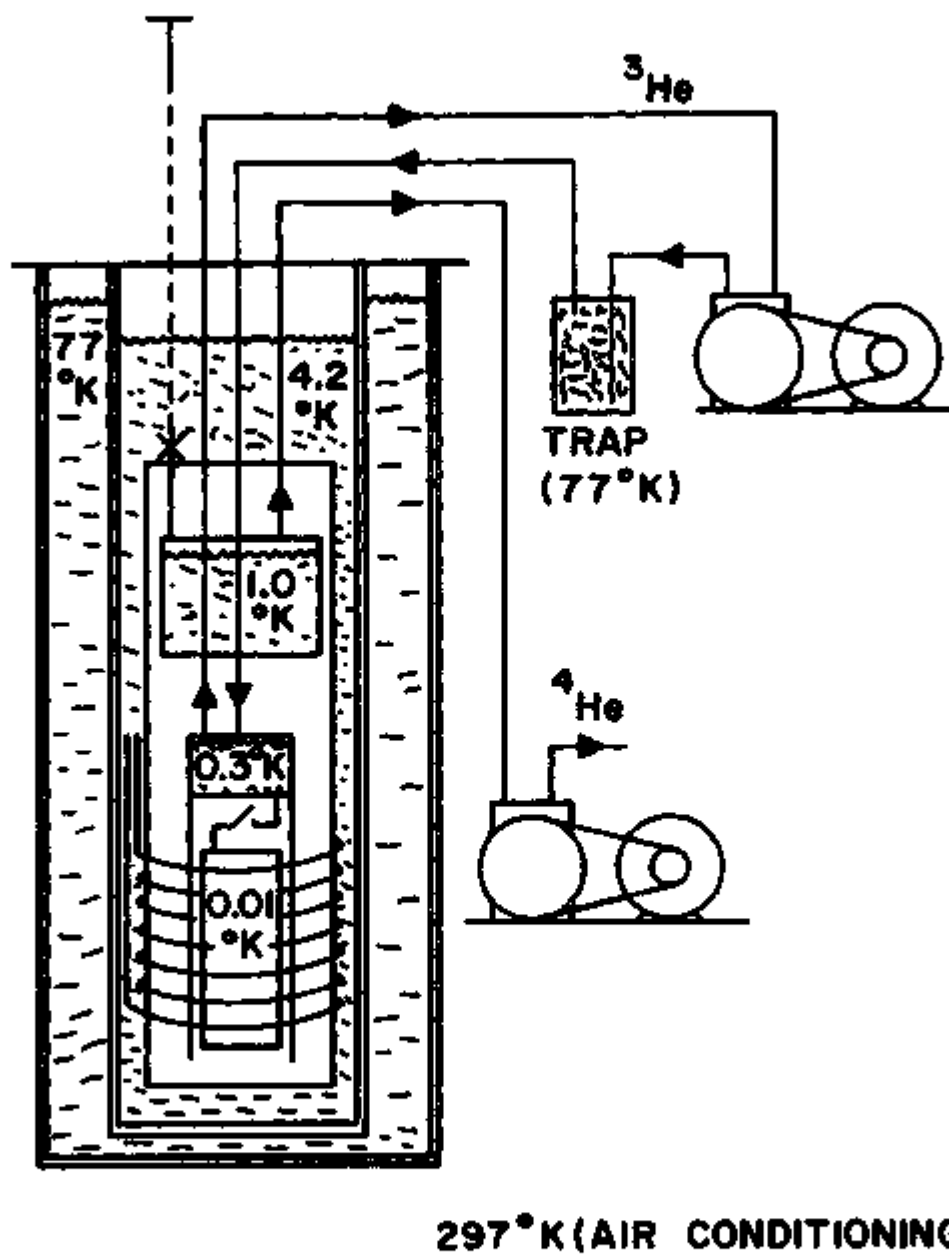
Figure 6. Block diagram of apparatus.

^{3}He PUMP LINE

^{4}He PUMP LINE

^{3}He RETURN LINE

VACUUM CAN PUMP LINE

CONDENSER

^{4}He FILL VALVE

PUMPING ORIFICE

IMPEDANCE

^{4}He EVAPORATOR 1°K

LEAD HEAT SWITCH

^{3}He EVAPORATOR 0.3°K

VACUUM CAN

SALT PILL

DEMAGNETIZING MAGNET

Cu FINS

He DEWAR

RADIATION SHIELD

He BATH

SAMPLE AND THERMOMETER

POLARIZING MAGNET
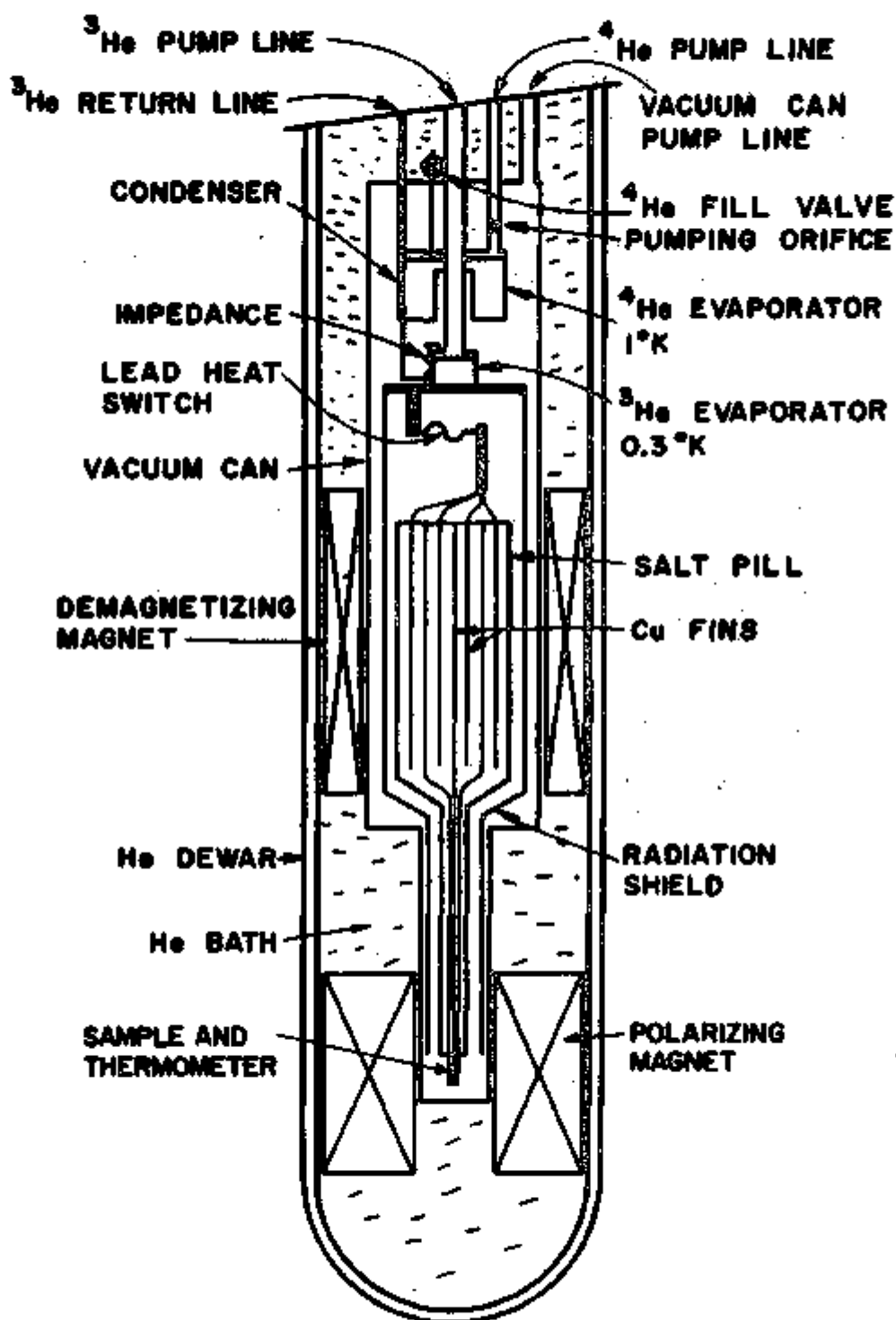
Figure 7.   Schematic of cryostat.

capillary. The pressure drop in the ^{3}He return line from 10 Torr at 1 K in the condenser to 10 mTorr at 1/3 K in the ^{3}He evaporator is provided by a length of capillary with a wire inside it which served as an impedance. Most of the capillary is in thermal contact with the ^{3}He evaporator. A radiation shield enclosing the salt pill to reduce the loading from thermal radiation is threaded onto the bottom of the ^{3}He evaporator. The thermal connection between the salt pill and the ^{3}He evaporator is a thin lead ribbon located in the fringing field of the demagnetizing magnet. As the salt pill is demagnetized, the lead goes super-conducting, thermally isolating the salt from the evaporator. The sample is located over 30 cm from the paramagnetic salt to reduce the field at the salt from the polarizing magnet. This field is a definite limitation to the temperature reached after demagneti-zation when we use our large polarizing magnet at high field values.

The gas handling system is shown in Figure 8. The ^{3}He system is a closed system with a sealed pump to avoid any leakage of ^{3}He out of the system or air into the system. The cost of ^{3}He prohibits its use in the same manner as ^{4}He. The ^{4}He system exhausts through a filter to a vent to the roof.

The polarizing magnet is a Magnion CF50 - 1-1/16 - 600 which we modified to fit into our 4-in. dewar system. It is 6 in. long with a 1-1/16-in. bore. A new persistent current switch was installed and the splices were remade and repositioned in order to avoid quenching at low field values in the new configuration.
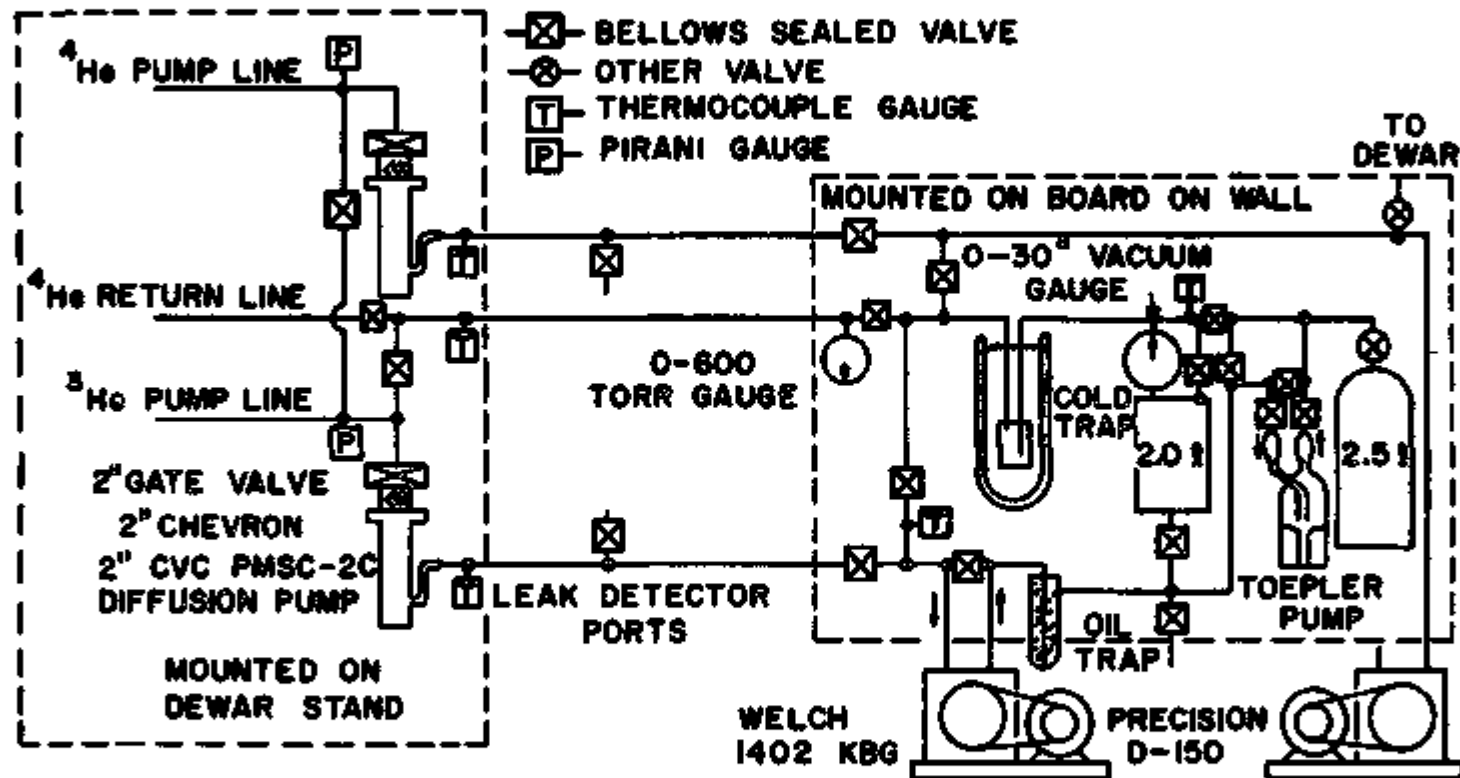
Figure 8. External gas handling system.

Calibration of the magnet with an F. W. Bell Model 610 gaussmeter
and a model A6131 axial Hall probe gave a value of 2.39 ± 0.01
kOe/A.[43] Since there is a 3 ohm protective shunt across the
magnet, the calibration for actual current through the magnet
rather than current indicated on the power supply was 2.46 ± 0.01
kOe/A. To avoid accidental quenching, the current in the magnet
was usually kept below 17.3 A corresponding to a field of 42.6 kOe
at the center of the magnet. The polarizing magnet was centered
1 in. below the sample to increase the distance to the salt pill.
The calculated field 1 in. from the center of the solenoid is
0.9807 times the field at the center.

The magnet used for saturating the paramagnetic salt was
manufactured by Westinghouse. It is 9-1/4 in. long with a
2.50-in. bore and is equipped with a persistent current switch.
The magnet has a rated field of 15 kOe at 18.4 A; however, we
usually operate it at 18 kOe with 22 A current.

The current for both superconducting magnets is supplied by
a Westinghouse 503B magnet controller. This transistorized unit
provides up to 25 A current with a RMS current ripple of less than
0.01%. It also supplies power for the persistent current switch
heaters. A switching box enables us to connect either magnet to
the current supply while leaving the protective shunts across the
magnets.

Detectors

Two different detector systems were used in this experiment.
During run 26 two scintillation detectors were used, one parallel
to the applied polarizing field and one perpendicular to it.
These detectors are referred to as the π and σ detectors
respectively after spectroscopic notation. In this way both $W(0)$
and $W(\pi/2)$ could be measured. By the time runs 27 and 28 were made
a solid state detector had been purchased, and it was used for its
much higher energy resolution. With only one detector $W(0)$ was
measured, since the change in $W(0)$ is usually larger than the
change in $W(\pi/2)$.

The scintillation detectors used were two Harshaw 12S12
integral line scintillation detectors with 3x3-in. NaI(Tl) crystals
and 3-in. RCA 8054 photomultiplier tubes. The pulse height
resolution of these detectors is better than 7½% at 662 keV. The
high voltage for the photomultipliers was supplied by a Fluke
model 402M power supply and two model 2901 photomultiplier voltage
dividers made by Sturrup Nuclear Division of Canberra Industries.
The photomultipliers were magnetically shielded by three concentric
layers of magnetic shielding; however, the polarizing magnet had a
large influence on the gain of the photomultiplier on the detector
parallel to the field. Every time the polarizing field was increased,
the gain on the linear amplifier for the π detector had to be
increased to compensate for the gain shift in the photomultiplier.

The data handling electronics are shown in Figure 9. The photomultipliers are connected to two Sturrup model 1405 charge sensitive preamplifiers then to two model 1415 RC amplifiers. The outputs of these amplifiers are connected both to a common model 1465 summing amplifier and to separate model 1432 integral discriminators. The summing amplifier is connected to a Victoreen SCIPP 400 multichannel pulse height analyzer. The integral discriminator outputs are used as routing pulses to put the spectrum from the σ detector in the first 200 channels of memory of the pulse height analyzer and the spectrum from the π detector in the second 200 channels. The memory of the analyzer can be read out on a model 33 Teletype, or it can be recorded on a Kennedy 1500 incremental tape recorder. The interface to the tape recorder was built in the department's electronic shop.

Our solid state detector was a lithium drifted germanium detector (Ge(Li) detector) manufactured by Canberra Industries. It is a 7000 Series 5-sided coaxial detector with an active volume of about 30 cm^3. The resolution of our detector was measured by Canberra to be 3.0 keV FWHM with a peak to Compton ratio of 16:1 and an efficiency of 4.3% relative to a 3x3-in. NaI(Tl) scintillation detector. These measurements were made on the 1.33 MeV peak of ^{60}Co.

The data handling system for the Ge(Li) detector was much less complicated than that for the NaI detectors since only one spectrum was collected and routing pulses were not used. A bias of

Ho

σ DETECTOR

SAMPLE AND
POLARIZING MAGNET

PRE-AMP

LINEAR AMPLIFIER

INTEGRAL DISCRIMINATOR
Channels 0 – 199

ROUTING SIGNAL

SUMMING AMPLIFIER

DATA SIGNAL

π DETECTOR

PRE-AMP

LINEAR AMPLIFIER

INTEGRAL DISCRIMINATOR
Channels 200–399

ROUTING SIGNAL

KENNEDY 1500 INCREMENTAL TAPE RECORDER

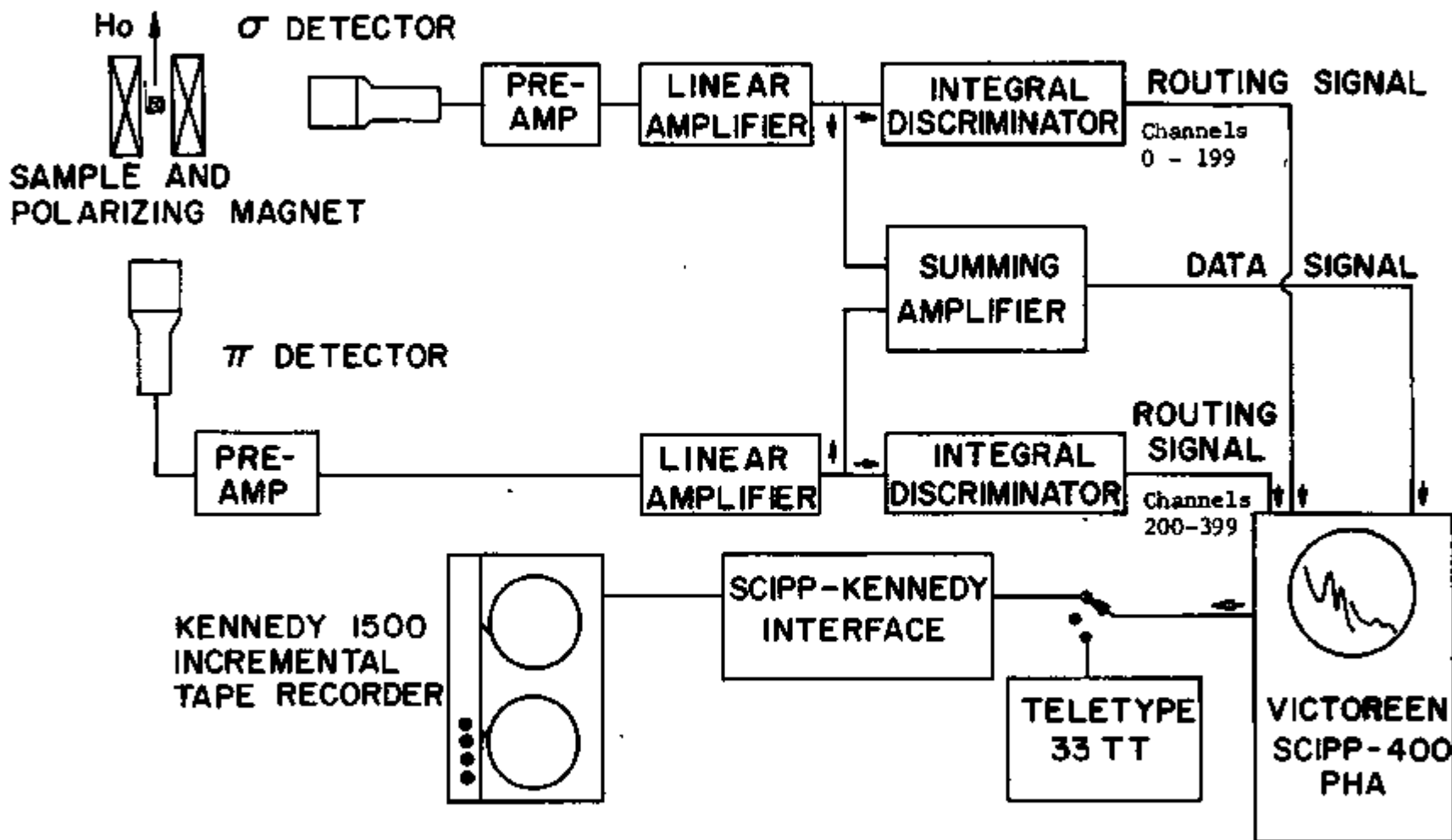SCIPP–KENNEDY INTERFACE

TELETYPE 33 TT

VICTOREEN SCIPP-400 PHA

Figure 9. Block diagram of electronics for scintillation detectors.

43

almost 1300 V is maintained by four 300+ V batteries. The charge
output signal from the detector is integrated and shaped by a
Canberra model 1408C spectroscopy preamplifier. The signal is then
amplified by a model 1416 spectroscopy amplifier and fed into the
pulse height analyzer. The output options are the same as in the
other system.

Preparation of Samples

The samples for the nuclear orientation runs were received
as 0.005-in. praseodymium foil from A. D. MacKay[44] in two
separate orders. The first order marked 99.9% showed considerable
surface oxidation. The second order was marked 99.9+% and had a
much cleaner surface. All samples were wet sanded using xylene
and 320 grit silicon carbide sandpaper until a clean surface was
obtained. The foils were then plated with aluminum by vacuum
evaporation to prevent corrosion during shipment to and from the
reactor. Praseodymium oxidizes rather rapidly at the least
provocation. As a further precaution the foils were shipped in a
nitrogen atmosphere in a small polyethylene bottle sealed with
vacuum grease. Each sample to be irradiated consisted of 8 or 10
pieces 8 by 16 mm by 0.10 to 0.12 mm thick after sanding. The
total weight of each sample was about 0.5 g. No weight gain to
0.0001 g could be measured after plating with aluminum. The
samples were exposed to a thermal neutron flux at the Research
Reactor Facility of the University of Missouri at Columbia,

Missouri. Between 10 and 60 mCi of ^{142}Pr was produced in the samples by the reaction ^{141}Pr + ^{1}n → ^{142}Pr. The samples were flown back to the University of Minnesota by air freight. Table 2 summarizes pertinent information on the samples.

Sample number	Run number	Source	Weight	Initial activity	Amount used
112	26	1st order	0.412 g	60 mCi	3/4
116	27	2nd order	0.506	30	4/5
117	28	2nd order	0.573	11	4/5

Table 2. Data on praseodymium samples.

Once the irradiated samples had decayed to an activity level that was safe to handle, they were tinned under a jet of helium gas using an ultrasonic soldering iron and cadmium-bismuth solder.[45] The Cd-Bi solder has been found to have much better thermal conductivity at low temperatures than the usual Sn-Pb soft solders.[46] Care was taken to avoid heating the foils much above the melting point of the solder as they blackened when heated too much. The entire operation was performed behind shielding by an experimenter using gloves with thin lead formed over them for protection from the rather high β flux. Eight tinned Pr foils each 8x8 mm were soldered to the fins of the salt pill using the same solder. Since there are six fins in the tail section of the salt pill, two foils were soldered on either side of the center four fins.

An iron foil of similar size with a small amount of ^{60}Co diffused into it was soldered between the center two Pr foils as a thermometer. The temperature of the iron foil can be calculated from the anisotropy of the γ rays emitted by the ^{60}Co nuclei dissolved in the iron. The arrangement Cu fin - Pr - Fe - Pr - Cu fin insured that the thermometer would not be cooled below the temperature of the Pr by direct contact to a Cu fin. The activity of the thermometer was about 1 μCi for run 26. A different thermometer with about 7 μCi activity was used for runs 27 and 28. The self-heating of the thermometer caused by absorption of the 0.3 MeV β's which precede the γ's from ^{60}Co is less than 1 erg/min/μCi. The heating in Pr from the 2.16 MeV β's which occur 96.3% of the time is over 6 times as great for the same activity. Also for the same number of observed γ's from both ^{60}Co and ^{142}Pr, the ^{142}Pr must be 13 times stronger to compensate for the number of decays which do not result in a γ. Therefore, the self-heating of the thermometer should not elevate its temperature significantly above that of the Pr.

Experimental Procedure

Two factors which make obtaining orientation data on ^{142}Pr difficult are the short half life and the large number of high energy β's for each observable γ. Early in a run the self-heating of the sample caused by absorption of the β's not only affected the lowest temperature we could achieve after demagnetization,

but also affected the warm-up rate after demagnetization. By the time the activity had decayed to a level at which we could reach our lowest temperatures, the low counting rate provided poor statistics even over one hour counting periods.

The heat capacity of our salt pill is approximately 3×10^4 ergs/mK at 10 mK.[42] If we consider 0.7 times the maximum energy to be the average energy of a β, for 2.16 MeV maximum β's the heat produced in a sample by absorption of these β's is about 9 μW/mCi. This heating rate will produce a temperature increase in our salt pill of 11 mK/hr/mCi.

The temperature of the sample after demagnetization of the salt pill can also be limited by self-heating if the heat produced in the sample is great enough to set up a thermal gradient in the link connecting it with the salt pill. The copper fins between the paramagnetic salt and the sample are about 30 cm long with a total cross sectional area of 0.2 cm^2. Assuming 10 mK as the temperature of the salt and ignoring the boundary resistance between the fins and the frozen slurry we can calculate the temperature of the sample with a given activity. Using the value of Anderson et al. for the thermal conductivity of copper at low temperatures,[47] the calculation indicates that in order to cool the sample below 25 mK the activity of the sample must be below 300 μCi.

As a limit on the other end of a run we find that we get little useful data after the activity of the sample is less than 10 μCi. This activity will produce the same number of γ's as

0.37 µCi of a substance in which each decay results in a γ.
With both of these considerations we can get useful data for
about 5 half lives or during about 4 days out of a run.

The general procedures for each run were quite similar. We
would have the sample irradiated to an activity level sufficiently
high to allow for possible delays in shipping or assembling the
apparatus. Once the sample arrived and had decayed to an activity
level that was safe to handle, we would mount the Pr foils on the
salt pill, fill the salt pill with slurry, and assemble the
apparatus. Tinning and mounting the samples and assembling the
apparatus usually took six to eight hours. Overnight the
apparatus was allowed to cool to liquid nitrogen temperature.
Liquid helium could be transferred as early as the day following
delivery if the activity was low enough to permit immediate handling.
The earliest the salt pill could usually be demagnetized was the
day after the initial helium transfer; however, sometimes a
demagnetization could be attempted the evening following the
initial transfer. If after demagnetization the sample could not
be cooled below about 25 mK which was necessary to observe an
anisotropy, the salt was remagnetized and another attempt was
made the following day. Once the activity was low enough for the
sample to be cooled below 25 mK, data was collected as the salt
pill warmed up. Early in a run counting periods as short as
10 minutes were used while towards the end of a run counting
periods of 60 minutes were necessary. Live time was used rather
than clock time to compensate for the dead time of the analyzer

which decreased as the sample decayed. Occasionally the field
of the polarizing magnet was changed so that we could collect
data at different values of applied field. About once every
24 hours, after the temperature of the sample had risen several
mK, we would remagnetize the salt pill and take several warm
counts for normalization as the salt was cooled to 0.3 K by the
^{3}He evaporator. We would then demagnetize it again and collect
more cold data before repeating the cycle. With this schedule we
could collect data, either cold counts or normalization data, more
than 20 hours out of a day. When warm counts were desired or a
series of counting periods at the same applied field value were
to be taken, the analyzer could be set for the length of the
counting period and it would automatically collect and record the
spectra and erase its memory between each spectra. However, if
the applied field had to be changed every few spectra, an operator
had to remain with the apparatus -- long into the night if necessary.

Run 26 -- Our first run with praseodymium was with sample
112 and the detector system using two NaI(Tl) scintillation
detectors. A relatively weak ^{60}Co in Fe thermometer was used
with an activity of only 1 µCi. The sample had been irradiated
to 60 mCi, and when we assembled the apparatus the ^{142}Pr activity
was still quite high. When we checked out the electronics of
the detector system, the ^{142}Pr peak concealled the ^{60}Co peaks from
the thermometer, but we assumed that they would appear as the
^{142}Pr decayed. Unfortunately as the ^{142}Pr decayed, what emerged

was a set of unresolved peaks which we later identified as coming from ^{182}Ta. Tantalum is a typical impurity in rare earth metals since it is used for crucibles for processing them. The ^{182}Ta peaks at 1.122, 1.189, 1.222, and 1.231 MeV obliterated the weaker ^{60}Co peaks at 1.173 and 1.332 MeV. The half life of ^{182}Ta, 115 days, is much greater than that of ^{142}Pr, and therefore we could not wait for it to decay as the ^{142}Pr would be long since gone by the time the ^{182}Ta was weaker than the ^{60}Co.

Run 27 -- By the second run with Pr we had acquired the solid state detector system. The solid state detector was capable of resolving the ^{182}Ta peaks from the ^{60}Co peaks. The sample was only irradiated to half the initial activity of sample 112. A more active thermometer was used with an activity of about 7 μCi. Sample 116 for this run was from a different batch from sample 112 used in run 26 and apparently had less Ta since no ^{182}Ta peaks were observed in this run. However, a thermal short in the apparatus prevented us from reaching low temperatures in the first half of the run. After disassembling and reassembling the apparatus in the middle of the run, we were able to collect data for only two days before the sample became too weak.

Run 28 -- Our final nuclear orientation run with ^{142}Pr proceeded without the difficulties of the earlier runs. Sample 117 was irradiated to 11 mCi, and again no peaks associated with ^{182}Ta were observed. We were able to collect data over a 5 day period. Our data represents 44 hours of cold counting periods plus an additional 21 hours of warm counts for normalization purposes.

CHAPTER IV

EXPERIMENTAL RESULTS

Scintillation Detector Data

The data collected with the NaI(Tl) scintillation detectors during run 26 showed a much larger anisotropy in the γ radiation than we had expected. Unfortunately, since the ^{60}Co peaks used for a thermometer were masked by peaks from a ^{182}Ta impurity, we could not calculate temperatures and were not able to compare the data to predictions from either model. Also preliminary analysis of the ^{142}Pr peaks revealed difficulties in fitting the warm counts to a decay curve. This fitting will be discussed in a succeeding section of this chapter. Some warm counts from the π detector were several standard deviations away from the expected decay curve casting considerable doubt on the reliability of the data. The large gain shifts in the photomultiplier of the π detector might be indicative of further problems in the detector even though the linear amplifier was able to compensate for the gain shift itself.

Run 26 was tantalizing in the size of the effect observed but disappointing in that the data did not allow comparison to theory.

Solid State Detector Data

The spectra from runs 27 and 28 were taken using a lithium drifted germanium detector. The resolution of this detector is shown in Figure 10. Since we were not using routing and were
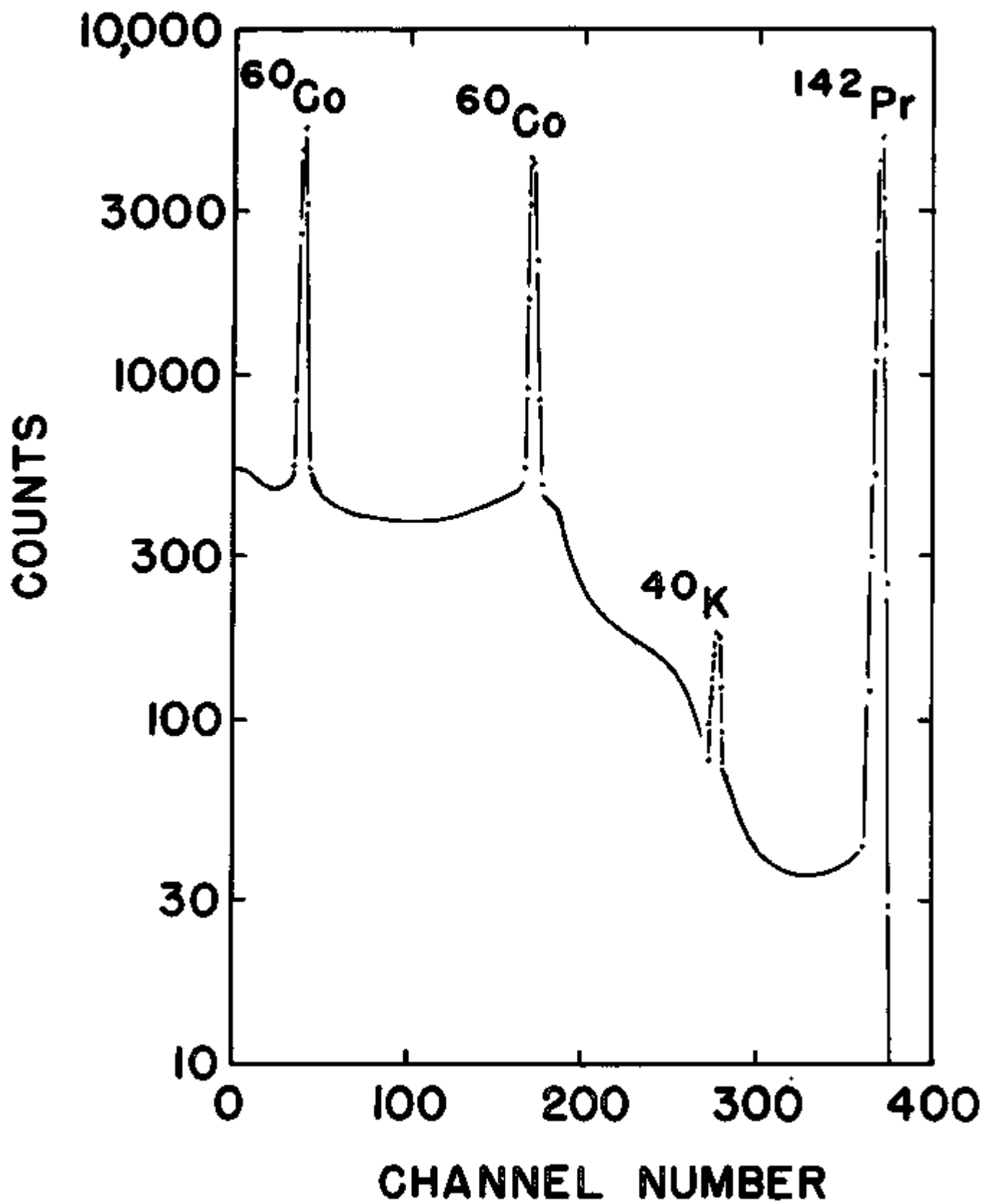
Figure 10. Typical Ge(Li) detector spectrum from run 28.

only using one detector, we could use the full 1600 channel ADC of the analyzer and select the 400 channel quadrant of interest to put into memory. In this way we could expand the area of interest to fit the 400 channel memory of the pulse height analyzer. The small peak between the ^{142}Pr peak and the higher energy ^{60}Co peak is caused by the naturally occurring isotope ^{40}K and is part of the room background.

The peaks in a Ge(Li) detector spectrum are not Gaussian in shape and cannot be fit by a computer to a Gaussian curve as is often done with scintillation detector spectra. However, the high resolution of the detector allows easy hand integration under the peaks with an electronic desk calculator. By making these calculations during a run, the values of applied field for subsequent data can be judiciously chosen. The number of counts in a peak was calculated by summing the counts in the 10 consecutive channels with the highest number of counts in the immediate vicinity of the peak. A background correction was made by subtracting half the sum of 20 channels — those 11 to 20 channels above the group summed for the peak and those 11 to 20 channels below the peak group. This correction had to be modified for the 1.33 MeV ^{60}Co peak because the Compton edge from the 1.57 MeV ^{142}Pr peak falls in one of the background counting regions. Therefore channels 3 to 12 above the peak group were substituted for those 11 to 20 above the peak group. An additional correction was made by taking a long background count in the room without the

sample or the thermometer in place and summing in the same manner
the channels where the peaks would have been. These corrections,
in counts per minute, were subtracted from the corresponding
integrals for the three peaks once they too had been converted
to counts per minute.

Decay Correction

The half life of ^{60}Co is 5.26 years. Over a period of a week
the activity of a sample of ^{60}Co will decrease by less than ½%.
Since the warm counts are averaged over an entire run, the decay
will affect the values of W(0) by less than ½%. This small an
effect will not seriously affect our temperatures calculated from
the ^{60}Co peaks; therefore, no decay corrections were made to the
^{60}Co peaks.

The short half life of ^{142}Pr makes a decay correction essential
for this isotope. The counting rate of each warm counting period
was plotted on semi-log graph paper as a function of the time
referenced to the middle of the counting period. A straight line
with a slope corresponding to a 19.2 hour half life was fitted
through the warm data points. Figure 11 shows such a plot for
run 28.

Small consistent deviations above or below the expected
straight line decay curve appearing near the end of a run indicate
respectively too little or too much background correction. Early
in a run the background corrections are very small compared to
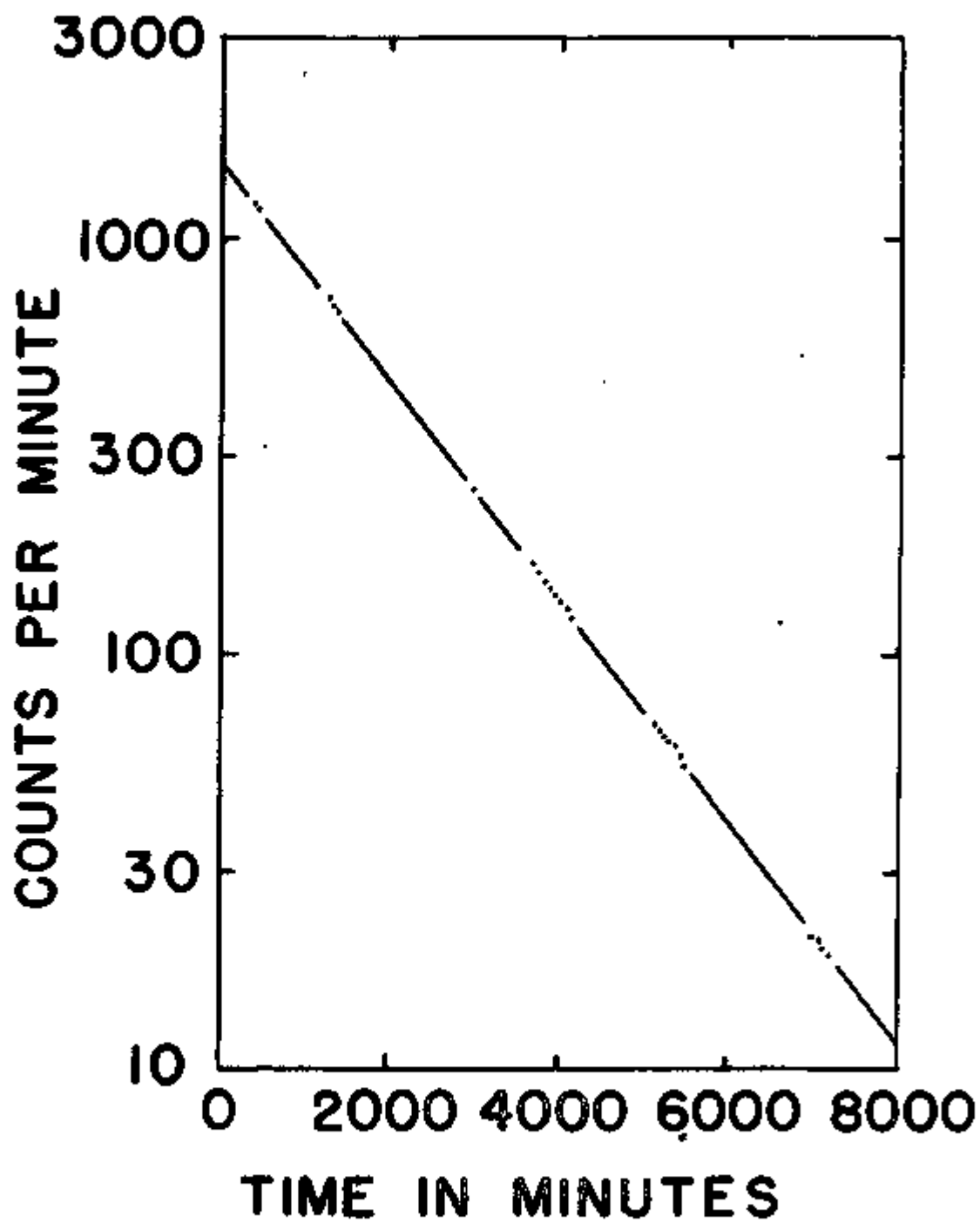the ^{142}Pr counting rate. Only late in the run, after the sample

Figure 11. Decay plot of warm counts from run 28.

has decayed to a relatively low activity, do they become
important. A linear deviation would indicate an incorrect half
life. To correct for such small deviations and to make a more
accurate fit to the warm data a computer fit to the data points
was made by varying the calculated counting rate at t=0 and also
a possible small extra background correction. The fit to data
points was weighted by the square root of the number of counts
contributing to that data point. The fitting procedure was
repeated for 19.1 and 19.3 hr half lives, but the best fit was
found for a 19.2 hr half life.

The value of $W(0)$ for a cold data point was calculated by
taking the ratio of the cold counting rate to the warm counting
rate at t=0 and multiplying this ratio by the decay factor
calculated at the middle of the counting period. The decay
factor is simply $\exp(-1662/t)$ where t is the time in minutes to the
middle of the cold counting period and 1662 is the number of
minutes for a ^{142}Pr sample to decay to $1/e$ times its initial
activity.

Solid Angle Correction

The detectors do not actually measure $W(0)$ or $W(\pi/2)$ but
$W(\theta)$ averaged over the effective solid angle subtended by the
detector. This effect can be taken into account by inserting
solid angle correction factors Q_2 and Q_4 into the expressions
for $W(\theta)$.

$$W(\theta) = 1 - Q_2 \epsilon_2 P_2 (\cos \theta) - Q_4 \epsilon_4 P_4 (\cos \theta) \qquad \text{IV-1}$$

All the other coefficients preceeding the Legendre polynomials have been lumped into ϵ_2 and ϵ_4. Tables of these correction factors as functions of energy and distance to sample have been caluclated by Yates for various standard NaI(Tl) detectors.[48] His values do not include sample to detector distances as large as those used in this experiment for our NaI(Tl) detectors and do not include values for solid state detectors. Therefore the expressions for Q_2 and Q_4 given by Rose were used.[49]

$$Q_2 = (1 + \mu)/2 \qquad \text{IV-2}$$

$$Q_4 = (1 + \mu)(7\mu^2 - 3)/8 \qquad \text{IV-3}$$

where μ is the cosine of the effective half angle subtended by the detector. The solid state detector was 22 cm from the sample and had a frontal area of 9.8 cm^2. The solid angle correction factors were calculated to be $Q_2 = 0.997$ and $Q_4 = 0.991$. These values are close enough to one to be ignored when the statistical error in our data is considered.

Calculation of Temperature

In runs 27 and 28, values of $W(0)$ were calculated as indicated in a previous section for each ^{60}Co peak. Since both peaks have the same anisotropy, an average of the values of $W(0)$ for the two peaks was taken and the corresponding value of

H_{int}/T was found on a graph of $W(0)$ as a function of H_{int}/T. The hyperfine field experienced by ^{60}Co nuclei in Fe is -287.7 kOe.[50] Therefore, the internal field, H_{int}, for ^{60}Co nuclei in an Fe foil saturated by an applied field, H_0, applied parallel to the foil is given by H_0-287.7 kOe. The temperature of the sample can be calculated by dividing H_0-287.7 by the value of H_{int}/T from the graph. A graph of $W(0)$ as a function of $1/T$ for ^{60}Co in Fe is shown in Figure 12. The statistics in the thermometer peaks contribute an error of about ½% to the temperatures.

Data

The statistical errors in the data points from runs 27 and 28 are between 1 and 3 percent. This uncertainty is quite large compared to the observed anisotropy of $W(0)$ which was not over 10 percent with our values of applied field and temperature. Therefore, data points at the same applied field and at similar temperatures were averaged to improve statistics. Each point was weighted by the reciprocal of the square of its standard deviation calculated from the counting statistics. The temperatures within an average varied by less than 1 mK, so the error in the temperature of the average is less than 1/2 mK.

The counting rates during the last two demagnetizations of run 28 were between 48 and 12 counts per minute. The background counting rate correction made by the computer fit to the warm counts of run 28 was 1.6 counts per minute. This correction is larger than the statistical error in the data points and, for
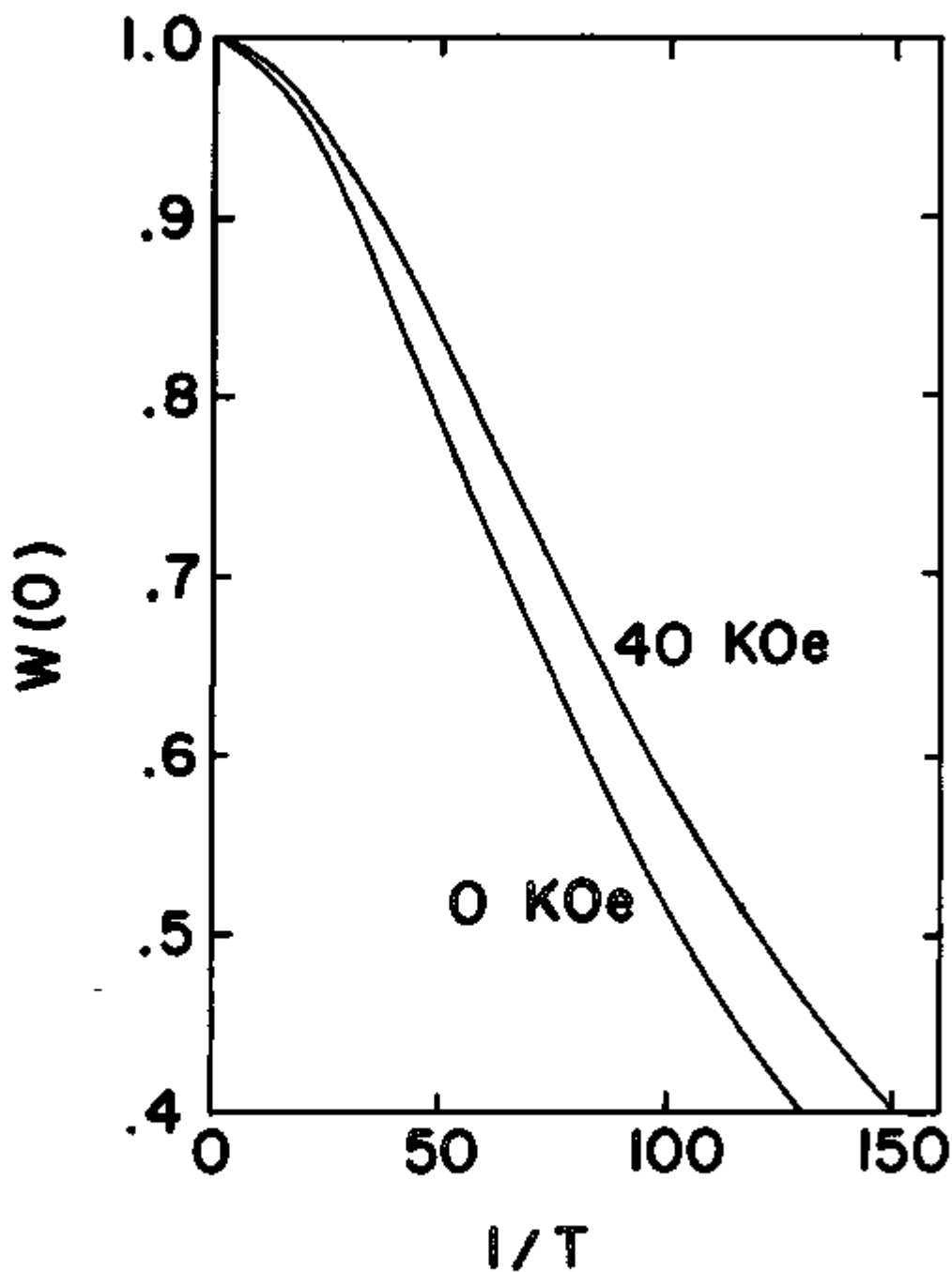
Figure 12. W(0) as a function of 1/T for ^{60}Co in Fe with applied fields of 0 and 40 kOe.

the last demagnetizations, becomes larger than the observed effect.
Therefore the data from the last two demagnetizations have not
been included in Table 3. Table 3 contains the values of $W(0)$
and temperature for the averages mentioned above. Data from
runs 27 and 28 have been included. The total number of counts
represented by each average is included in order to indicate the
statistical error in $W(0)$.

H_0 (kOe)	T(mK)	$W(0)$	Counts
41.7	20.7	.970	59060
41.7	16.4	.944	9618
41.7	15.1	.942	15762
41.7	12.2	.912	18428
28.8	15.7	.959	23419
28.8	12.3	.939	11347
20.5	15.4	.972	34376
20.5	12.8	.950	10506
14.3	13.1	.970	22982

Table 3. Averaged values of $W(0)$ from runs
27 and 28.

Discussion

In Figure 13 the average values of $W(0)$ from Table 3 have
been plotted as a function of H_0/T and compared to various
possible predictions based on the moment induced on the ground
state singlet of the crystal field energy levels by an applied
field. Since $W(0)$ is a function of H_{int}/T, if the internal field
is proportional to the applied field, the data points plotted as a
function of H_0/T should all lie along the same curve. However,
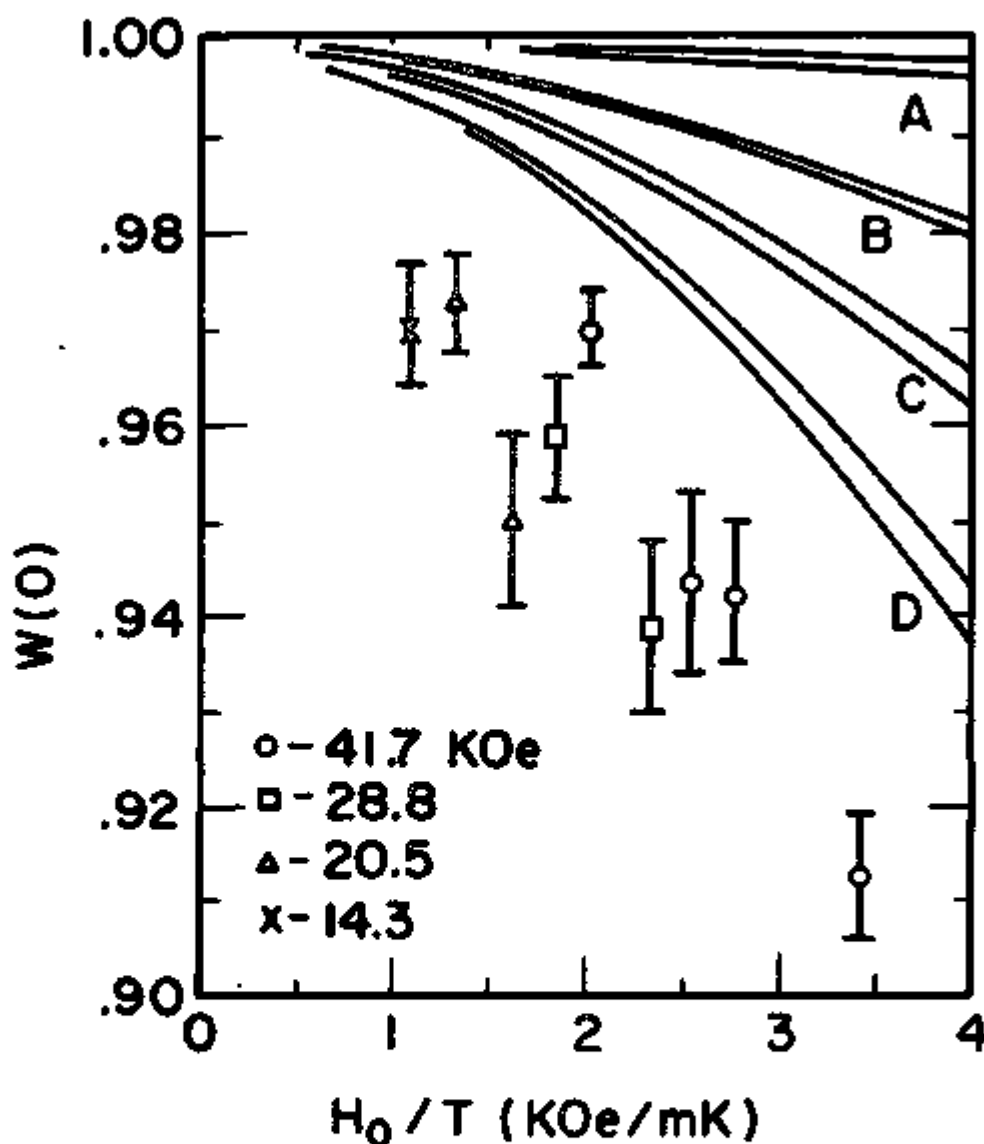
Figure 13. Comparison of data to predictions of crystal
  field model.
  Pair A -- hexagonal site ordered, 90 k splitting on
  cubic site. Upper curve $V/Y = -0.2$, lower curve
  $V/Y = -2.7$.
  Pair B -- cubic site ordered, 26 K splitting on hexagonal
  site, contributions averaged over (001) directions,
  $V/Y = -0.2$. Upper curve 41.7 kOe applied field, lower
  curve 14.3 kOe.
  Pair C -- same as B except $V/Y = -2.7$.
  Pair D -- same as C except no averaging over (001)
  directions -- single crystal.

if saturation of the moment causes smaller enhancement factors for
larger values of applied field, separate curves must be drawn for
each value of H_0.

The pair of curves labeled A at the top of the graph in
Figure 13 correspond to the assumption that the hexagonal sites
are ordered antiferromagnetically and the splitting between the
ground state singlet on the cubic site and the first excited state
is 90 K. Two curves are plotted for the two possible values of
V/Y. The denominator in Equation II-5 does not significantly
differ from one for this splitting and our values of H_0; therefore,
all values of H_0 have the same enhancement factor. Obviously this
model does not come close to accounting for the effect observed.

The other curves in Figure 13 are calculated from the
crystal field model with the cubic sites ordering antiferromagneti-
cally and a 26 K splitting between the ground state singlet on the
hexagonal site and its first excited state. The effect of the
deviation of the denominator in Equation II-6 from one is shown by
the slight displacement between the curves for $H_0=14.3$ kOe and for
$H_0=41.7$ kOe in the sets of curves labeled B, C, and D. For curves
B corresponding to $V/Y=-0.2$ and curves C corresponding to $V/Y=-2.7$,
contributions from the hexagonal sites have been averaged over
possible (001) directions as described in Chapter II. This
averaging should be necessary for the hexagonal site of a poly-
crystalline sample. Again the predicted effect is not as large as

the measured effect. Even assuming that the sample acts as a single crystal with $V/Y=-2.7$, as is shown in the curves labeled D, does not predict a large enough effect. The possible contribution from the cubic site, as indicated by the curves labeled A, is small enough so that assuming that the antiferromagnetic ordering is destroyed by an applied field and both sites contribute to $W(0)$ will not produce a large enough change to fit the data.

The values of $W(0)$ predicted from the moments measured by neutron diffraction work on a single crystal of Pr are shown in Figure 14 for $V/Y=-0.2$ and in Figure 15 for $V/Y=-2.7$. The contributions to $W(0)$ from the hexagonal sites have been averaged over the possible (110) directions and the contributions from the cubic sites have not been averaged as was discussed in Chapter II. The departure from a linear relationship between H_0 and H_{int} which is apparent from the curvature in the plots of ν as a function of H_0 in Figure 2 also results in definite separation of the curves of $W(0)$ as a function of H_0/T for different values of H_0 in Figures 14 and 15.

The set of curves for $V/Y=-0.2$ do not provide a satisfactory fit to the data as is shown in Figure 14. A deviation plot which graphs the ratio of the experimental value of $W(0)$ to the theoretical values as a function of H_0/T has been included to make the deviation of experimental values from predicted values clearer. The curves shown in Figure 15 for $V/Y=-2.7$, however, fit the data reasonably well considering the statistical error in the data.

Figure 14. Comparison of data to predictions calculated from moments measured by neutron diffraction. $V/Y = -0.2$. Deviation plot shows $W(0)_{exp}/W(0)_{theory}$.
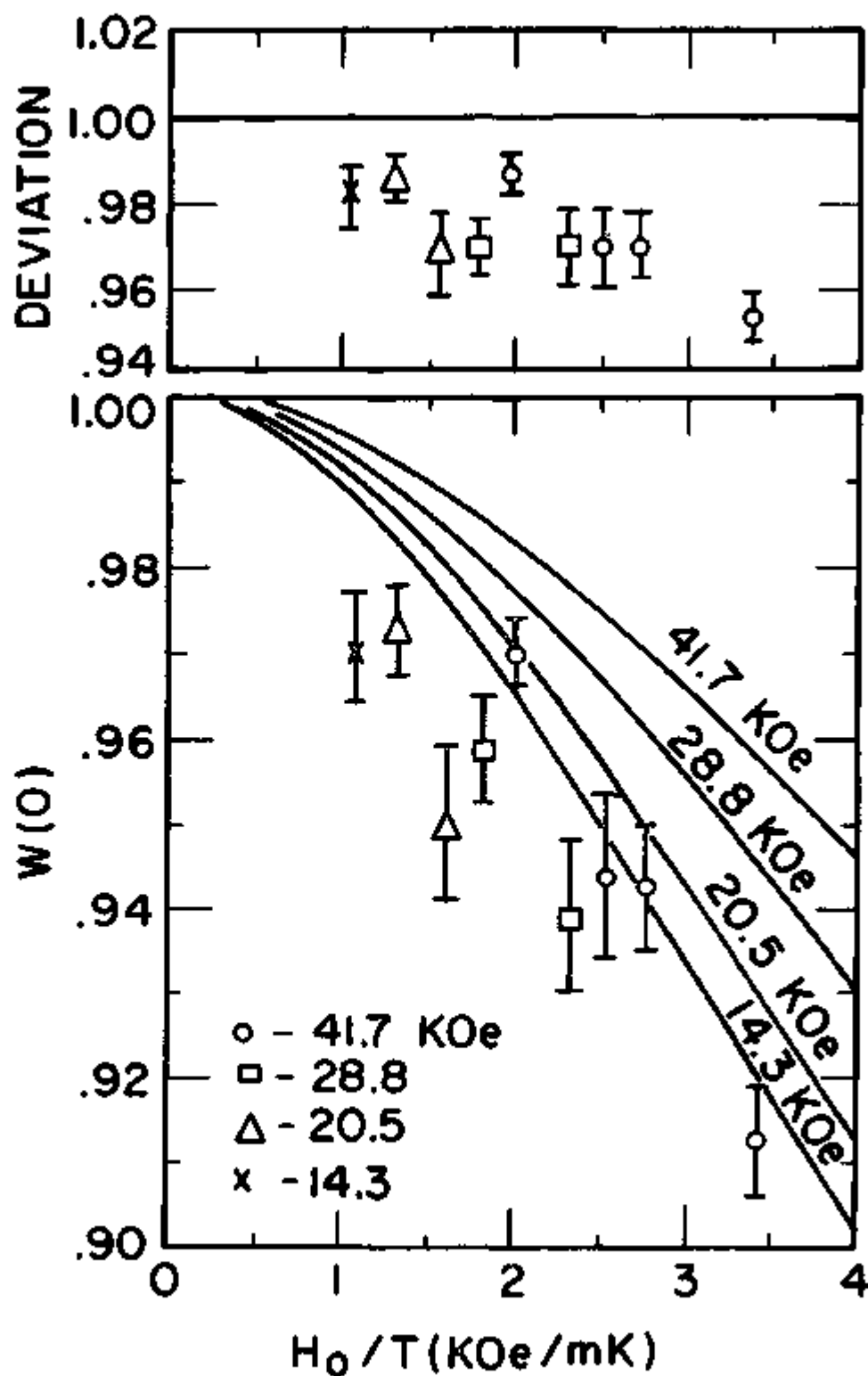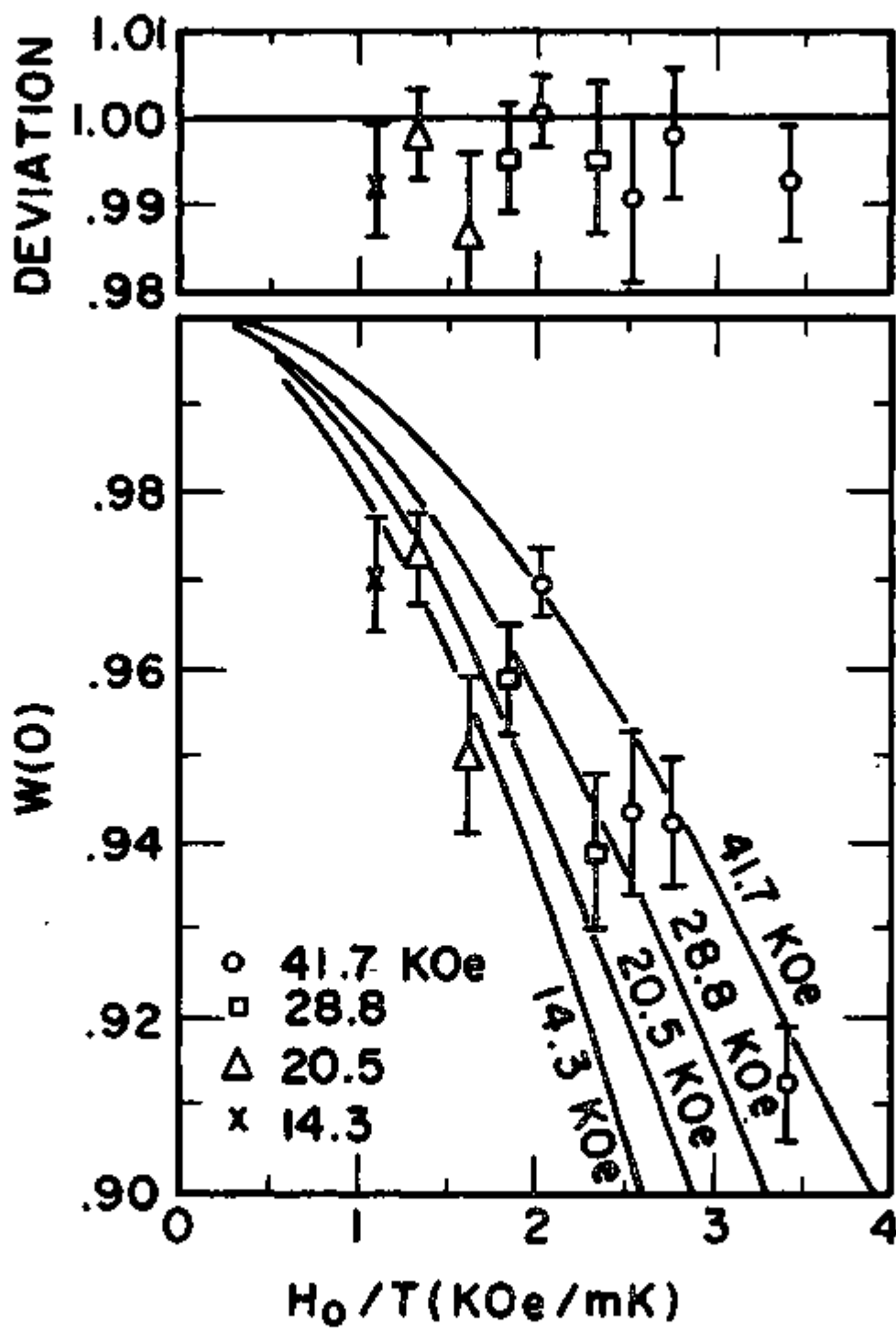
Figure 15. Comparison of data to predictions calculated from moments measured by neutron diffraction. $V/Y = -2.7$. Deviation plot shows $W(0)_{exp}/W(0)_{theory}$.

The deviation plot shows the anisotropy in $W(0)$ still slightly larger than the predicted effect. This remaining discrepancy could be due either to a slightly larger value of $|V/Y|$ or to contributions to the powder average from the small moment which Lebech and Rainford found on the hexagonal sites for an applied field parallel to the c axis.[9]

CHAPTER V

CONCLUSIONS

Despite the fact that we used a polycrystalline sample, our data appears to support the results of the neutron diffraction studies done on single crystal praseodymium.[8,9] Using the internal fields corresponding to the moments induced on the cubic and hexagonal sites as measured by Lebech and Rainford[9] and a model with neither sites ordered, we were able to calculate values of $W(0)$ which agree reasonably well with our data. It is doubtful that either site in our sample remained antiferromagnetically ordered in our applied fields since an antiferromagnetic site reduces the total possible anisotropy of γ radiation from the sample. Apparently our applied fields were large enough to destroy the antiferromagnetic order which was observed by neutron diffraction studies on polycrystalline Pr metal.[7]

The anisotropies predicted by using the moment induced by an external field on the ground state singlet of either site are much too small to explain our data if the energy splittings inferred from specific heat measurements are used. Even if neither site orders the effect is too small. Since the crystal field inter-actions are so similar in size to the exchange forces that there can be differences in ordering between single crystal and

polycrystalline samples, possibly using the crystal field eigenfunctions and energy levels to calculate the moments induced on the sites is not legitimate. The magnetic ordering of Pr is odd enough that it has been suggested that the usual technique of treating the ordering interactions as an effective molecular field is inadequate. Rainford claims that inelastic neutron scattering measurements he and J. C. G. Hounmann are making suggest that molecular field treatment is inappropriate for the low temperature magnetic properties of Pr.[51]

Additional neutron diffraction studies of polycrystalline samples of Pr in an applied field would hopefully determine whether the disruption of the antiferromagnetic order is sudden or gradual as the applied field is increased and what applied field is necessary to break up the ordered state. Magnetization studies comparing polycrystal and single crystal samples at liquid helium temperatures could also shed some light on the moment induced on the two sites. The magnetization data by Henry appears to differ by a factor of 2 from the moments derived from single crystal neutron diffraction.[52] Specific heat data in an applied field may reveal the order-disorder transition and whether the destruction of the ordering is temperature and field dependent. Some preliminary work on measuring the specific heat of polycrystalline Pr in a magnetic field at temperatures above 5 mK has been started in this laboratory.

A second result of our experiment is the selection of one of the two possible ratios of matrix elements indicated by β-γ circular polarization correlation measurements. The size of the anisotropy we observed can only be accounted for by V/Y=-2.7. For an independent determination of V/Y, nuclear orientation measurements of ^{142}Pr in a host with only one environment should be made. The value of V/Y can be calculated from values of B_2 and B_4. The alloy PrBi with its cubic rock salt structure may lend itself to such a study.

Finally the relatively large orientation of the ^{142}Pr nuclei despite their small nuclear moment indicates a large internal field can be achieved with a rather small applied field. Such a system should be ideal for nuclear cooling by adiabatic demagnetization. Cooling of the sample upon reduction of the polarization field has been observed in this laboratory. Hyperfine enhanced nuclear magnetic cooling has also been observed by Andres and Bucher in the alloy PrBi.[53] PrBi also has a singlet ground state on which an external field can induce a large moment.

The magnetic structure of praseodymium metal may yet have some interesting surprises to be revealed by careful study of its magnetic properties.

FOOTNOTES

1. R. J. Elliot, in *Magnetism* Vol. IIA, edited by G. T. Rado and H. Suhl (Academic Press, New York, 1965), p. 385.

2. O. V. Lounasmaa, Phys. Rev. *133*, A212 (1964).

3. B. Holmström, A. C. Anderson, and M. Krusius, Phys. Rev. *188* 888 (1969).

4. B. Bleaney, Proc. Roy. Soc. (London) *A276*, 39 (1963).

5. W. E. Wallace, F. Kessesl, E. Segal, and R. S. Craig, J. Phys. Chem. Solids *30*, 13 (1969).

6. Y. Kubota and W. E. Wallace, J. Appl. Phys. *34*, 1348 (1963).

7. J. W. Cable, R. M. Moon, W. C. Koehler, and E. O. Wollan, Phys. Rev. Letters *20*, 553 (1964).

8. J. Johansson, B. Lebech, N. Nielsen, H. Bjerrum Møller, and A. R. Mackintosh, Phys. Rev. Letters *25*, 524 (1970).

9. B. Lebech and B. D. Rainford, paper submitted to the Grenoble Magnetism Conference (1970).

10. F. H. Spedding, A. H. Daane, and K. W. Herrmann, Acta Cryst. *9*, 559 (1956).

11. K. A. Gschneidner, Jr., in *The Rare Earths*, edited by F. H. Spedding and A. H. Daane (John Wiley and Sons, New York, 1961), p. 190.

12. R. M. Moon, J. W. Cable, and W. C. Koehler, J. Appl. Phys. *35*, 1041 (1964).

13. H. Nagasawa and T. Sugawara, J. Phys. Soc. Japan *23*, 701 (1967).

14. E. Bucher, C. W. Chu, J. P. Maita, K. Andres, A. S. Cooper, E. Buehler, and K. Nassau, Phys Rev. Letters *22*, 1260 (1969).

15. C. W. Dempsey, J. E. Gordon, and T. Soller, Bull. Am. Phys. Soc. *7*, 309 (1962).

16. J. M. Lock, Proc. Phys. Soc. (London) *B70*, 566 (1957).

17. D. A. Parkinson, F. E. Simon, and F. H. Spedding, Proc. Roy. Soc. (London) A207, 137 (1951).

18. B. Grover, Phys. Rev. 140, A1944 (1965).

19. A. J. Freeman and R. E. Watson, in Magnetism Vol. IIA, edited by G. T. Rado and H. Suhl (Academic Press, New York, 1965), pp. 168-305.

20. J. Kondo, J. Phys. Soc. Japan 16, 1690 (1961).

21. R. E. Watson and A. J. Freeman, in Hyperfine Interactions, edited by A. J. Freeman and R. B. Frankel (Academic Press, New York, 1967), p. 69.

22. O. V. Lounasmaa, in Hyperfine Interactions, edited by A. J. Freeman and R. B. Frenkel (Academic Press, New York, 1967), p. 484.

23. P. G. E. Reid, N. J. Stone, H. Bernas, D. Spanjaard, and I. A. Campbell, Proc. Roy. Soc. (London) A311, 169 (1969).

24. E. Ambler, Progress in Cryogenics 2, 235 (1960).

25. R. J. Blin-Stoyle and M. A. Grace, Handbuch der Physik Vol XLII, edited by S. Flugge (Springer-Verlag, Berlin, 1957), pp. 555-610.

26. S. R. de Groot, H. A. Tolhoek, and W. J. Huiskamp, in Alpha-, Beta-, and Gamma-Ray Spectroscopy Vol. 2, edited by K. Siegbahn (North-Holland Publishing Co., Amsterdam, 1965), pp. 1199-1266.

27. J. M. Daniels, Oriented Nuclei: Polarized Targets and Beams (Academic Press, New York, 1965).

28. J. A. M. Cox and H. A. Tolhoek, Physica 19, 101 (1953).

29. C. D. Hartogh, H. A. Tolhoek, and S. R. de Groot, Physica 20, 1310 (1954).

30. U. Fano, Nuovo Cimento 5, 1358 (1857).

31. M. E. Rose, Elementary Theory of Angular Momentum (John Wiley and Sons, Inc., New York, 1957), pp. 107-124.

32. L. C. Biedenharn, J. M. Blatt, and M. E. Rose, Rev. Mod. Phys. 24, 249 (1952).

33.   T. Kotani and M. Ross, Phys. Rev. Letters 1, 140 (1958).

34.   T. Kotani and M. Ross, Phys. Rev. 113, 622 (1959).

35.   H. A. Weidenmüller, Rev. Mod. Phys. 33, 574 (1961).

36.   F. M. Pipkin, J. Sanderson, and W. Weyhmann, Phys. Rev. 129, 2626 (1963).

37.   T. Kotani, Phys. Rev. 114, 795 (1959).

38.   R. M. Steffen, Phys. Rev. 123, 1787 (1961).

39.   C. S. Wu and S. A. Moszkowski, Beta Decay (Interscience Publishers, New York, 1966), p. 59.

40.   C. M. Lederer, J. M. Hollander, and I. Perlman, Table of Isotopes 6th Edition (John Wiley and Sons, Inc., New York, 1957), p. 291.

41.   R. Hess, P. Lipnik, Chs.-Fs. Perdrisat, and J. W. Sunier, Nuclear Phys. 54, 673 (1964).

42.   C. H. Smith and W. Weyhmann, Adiabatic Demagnetization Cryostat for Thermal Equilibrium Nuclear Orientation, AEC Report COO-1569-35 (1968).

43.   The calibration data was taken by Jim Holliday using a cryostat designed by Robert Swinehart which allowed room temperature access to the center of the magnet.

44.   A. D. MacKay Inc., 198 Broadway, New York, N.Y. 10038.

45.   This solder is a 60% bismuth-40% cadmium eutectic alloy manufactured by Semi-Alloys Inc., 20 N. MacQuesten Parkway, Mount Vernon, N.Y.

46.   W. A. Steyert, Rev. Sci. Instr. 38, 964 (1967).

47.   A. C. Anderson, G. L. Salinger, and J. C. Wheatley, Rev. Sci. Instr. 32, 1110 (1961).

48.   M. J. L. Yates, in Perturbed Angular Correlations, edited by E. Karlsson, E. Matthias, and K. Siegbahn (North-Holland Publishing Company, Amsterdam, 1964), pp. 453-466.

49.   M. E. Rose, Phys. Rev. 91, 610 (1953).

50. D. A. Shirley, in _Hyperfine Structure and Nuclear Radiations_, edited by E. Matthias and D. A. Shirley (North-Holland Publishing Company, Amsterdam and John Wiley & Sons, Inc., New York, 1968), p. 980.

51. B. D. Rainford (Private communication).

52. W. E. Henry, in _Proceedings of the Fourth Conference on Rare Earth Research_, edited by LeRoy Eyring (Gordon and Breach, New York, 1965), p. 38.

53. K. Andres and E. Bucher, Phys. Rev. Letters $\underline{21}$, 1221 (1968).